JOURNAL OF PETROLOGY | VOLUME 44 | NUMBER 5 | PAGES 867–900 | 2003

Temperatures of Granulite-facies Metamorphism: Constraints from Experimental Phase Equilibria and Thermobarometry Corrected for Retrograde Exchange

DAVID R. M. PATTISON[1]*, THOMAS CHACKO[2], JAMES FARQUHAR[3] AND CHRISTOPHER R. M. McFARLANE[4]

[1]DEPARTMENT OF GEOLOGY AND GEOPHYSICS, UNIVERSITY OF CALGARY, CALGARY, AB, T2N 1N4, CANADA

[2]DEPARTMENT OF EARTH AND ATMOSPHERIC SCIENCES, UNIVERSITY OF ALBERTA, EDMONTON, AB, T6G 2E3, CANADA

[3]DEPARTMENT OF GEOLOGY AND EARTH SYSTEM SCIENCE INTERDISCIPLINARY CENTRE, UNIVERSITY OF MARYLAND, COLLEGE PARK, MD 20742, USA

[4]DEPARTMENT OF GEOLOGICAL SCIENCES, THE UNIVERSITY OF TEXAS AT AUSTIN, AUSTIN, TX 78701, USA

RECEIVED MAY 29, 2002; ACCEPTED NOVEMBER 18, 2002

This study assesses temperatures of formation of common granulites by combining experimental constraints on the P–T *stability of granulite-facies mineral associations with a garnet–orthopyroxene (Grt–Opx) thermobarometry scheme based on Al-solubility in Opx, corrected for late Fe–Mg exchange. We applied this scheme to 414 granulites of mafic, intermediate and aluminous bulk compositions. Our findings suggest that granulites are much hotter than traditionally assumed and that the* P–T *conditions of the amphibolite–granulite transition portrayed in current petrology textbooks are significant underestimates by over 100°C. For aluminous and intermediate granulites, mean corrected temperatures based on our method are 890 ± 17 and 841 ± 11°C, respectively (uncertainties reported as 95% confidence limits on the mean), consistent with minimum temperatures for orthopyroxene production by fluid-absent partial melting in these bulk compositions. In contrast, mean temperatures based on Grt–Opx Fe–Mg exchange equilibria, using the same thermodynamic data, are 732 ± 22 and 723 ± 11°C, respectively, well below the minimum temperatures for Opx stability. For mafic granulites, the mean corrected temperature using our method is 816 ± 12°C, similar to the mean temperature of 793 ± 13°C from Fe–Mg exchange. Reasons for the differences between the mafic granulites and aluminous–intermediate granulites are unclear but may be due to the lower Al concentrations in Opx in the mafic rocks and possible deficiencies in the thermodynamic modelling of these low concentrations. We discuss a number of well-known granulite terrains in the context of our findings, including the Adirondacks, the Acadian granulites of New England, the incipient charnockites of southern India and Sri Lanka, and the Kerala Khondalite Belt. Our findings carry implications for thermotectonic models of granulite formation. A computer program to perform our thermobarometry calculations, RCLC, is available from the* Journal of Petrology *website at http://www.petrology.oupjournals.org or from the authors at http://www.geo.ucalgary.ca/~pattison/drm_pattison-rclc.htm.*

KEY WORDS: *granulite-facies metamorphism; thermobarometry; garnet; orthopyroxene*

*Corresponding author. Telephone: 403-220-3263. Fax: 403-284-0074. E-mail: pattison@ucalgary.ca

INTRODUCTION

Although thermobarometric studies of granulite terrains have been carried out for more than 30 years, the temperatures reported in many of these studies fundamentally disagree with fluid-absent experimental data delimiting the stability of granulite-facies mineral assemblages. This discrepancy can be attributed to one of two primary causes (e.g. Nair & Chacko, 2002): (1) granulite metamorphism is triggered by the influx of low-a_{H_2O} fluids, which allows anhydrous minerals such as orthopyroxene to form at temperatures well below those required under fluid-absent conditions; or (2) peak temperatures of granulite metamorphism are higher than indicated by commonly used granulite geothermometers because of compositional re-equilibration of minerals on cooling. Although low-a_{H_2O} fluid infiltration has been inferred in a few granulite terrains (e.g. Janardhan *et al*., 1982; Chacko *et al*., 1987; Pattison, 1991; Bradshaw *et al*., 1989*b*; Todd & Evans, 1994), most granulites are thought to have formed under fluid-absent conditions (e.g. Harley, 1989; Thompson, 1990; Valley *et al*., 1990; Clemens, 1992; Spear *et al*., 1999). Thus, the temperature discrepancy noted above must be attributed to the inability of the minerals to retain their peak-temperature compositions.

Resetting of temperatures is related to the diffusional mobility of elements on which conventional granulite thermobarometry is based. Table 1 lists diffusion coefficients and length-scales of diffusion (diffusion penetration distances) for some major elements in common minerals, calculated for 850°C and 10 Ma. The diffusion penetration distances vary over six orders of magnitude in a predictable fashion according to crystal chemical constraints (Dowty, 1980), and suggest that there is little reason to expect simultaneous closure of elements at any point in a high-grade rock's P–T history, let alone at peak P–T conditions. Apart from the obvious implications for temperature, variable closure temperature also affects pressure estimates because these depend on the temperature [the 'feedback' effect of Harley (1989)].

Many granulite temperature estimates in the literature are based on Fe–Mg fractionation between coexisting phases such as garnet, biotite, cordierite, orthopyroxene and clinopyroxene [Grt, Bt, Crd, Opx, Cpx; abbreviations of Kretz (1983)]. Several studies have provided evidence that the closure temperature for Fe–Mg exchange between these phases is below peak granulite-facies temperatures (e.g. O'Hara, 1977; Lasaga, 1983; Frost & Chacko, 1989; Harley, 1989; Spear & Florence, 1992; Fitzsimons & Harley, 1994; Pattison & Bégin, 1994*a*, 1994*b*; Chacko *et al*., 1996). Pattison & Bégin (1994*a*, 1994*b*) suggested that, except for touching Fe–Mg minerals that continue to exchange Fe and Mg locally down to low temperatures, closure of intergranular Fe–Mg exchange may be controlled primarily by loss of a pervasive intergranular transport medium (probably melt), rather than by different rates of volume diffusion. In addition to these closure-related issues, a further complication arises if retrograde net-transfer reactions have taken place (Spear & Florence, 1992; Kohn & Spear, 2000). These can cause a variety of changes to the mineral compositions that can lead to erroneously high or low temperature estimates depending on what parts of the minerals are analyzed.

Focusing on the primary problem of closure temperature, two important questions are: (1) is the amount of retrograde Fe–Mg exchange below peak granulite conditions generally modest (e.g. <50°C) or substantial (e.g. >100°C)? (2) If it is substantial, what methods can be used to see through its effects to infer peak granulite P–T conditions? The first question has been addressed by kinetic modelling studies (e.g. Chakraborty & Ganguly, 1991; Spear & Florence, 1992; Ganguly & Tirone, 1999), but the results have been equivocal owing to uncertainties in the diffusion data and their extrapolation to natural conditions (e.g. Pattison & Bégin, 1994*a*, p. 388). The approach in this paper is to use constraints from experimental phase equilibria in concert with a geothermobarometry scheme based on Al-solubility in Opx in equilibrium with garnet, corrected for late Fe–Mg exchange, which we have applied to 414 Grt + Opx + Pl + Qtz-bearing

Table 1: Diffusion coefficients and diffusion length scales

Element and mineral	Reference	$\log_{10} D$ (cm^2/s) at 850°C, 10 kbar	Diffusion penetration distance* (mm), 10 Myr
Al in plagioclase	1	−23·0	0·001
Al in clinopyroxene	2	−19·3	0·08
Ca–Mg in clinopyroxene	3	−19·2	0·09
Fe–Mg in garnet	4	−16·2	3·00
Fe–Mg in orthopyroxene	5	−15·6	5·93
Fe–Mg in cordierite	6	−13·5	63·1
Na–K in plagioclase	7	−12·1	330·2

*Diffusion penetration distance $\sim(4Dt)^{0.5}$, where D is diffusion coefficient and t is time.
References: 1, Grove *et al*. (1984); 2, Jaoul *et al*. (1991); 3, Brady & McAllister (1983); 4, Chakraborty & Ganguly (1991); 5, Ganguly & Tazzoli (1994); 6, Lasaga *et al*. (1977); 7, Foland (1974), Brady & Yund (1983) and Yund (1986).

rocks from 62 granulite terrains worldwide. Whereas this combined approach has been used by Harley (1998*a*, 1998*b*) in his studies of ultra-high-temperature metamorphism, our focus is on the less exotic but more widespread 'ordinary' granulites of common mineralogy. Our results suggest that commonly reported temperatures of granulite-facies metamorphism are significant underestimates, on average by $>100°C$. We discuss several well-known granulite terrains in the context of our findings, including the Adirondacks, the Acadian metamorphic high of Massachusetts, the incipient charnockites of southern India and Sri Lanka, and the Kerala Khondalite Belt. We then explore the implications of these higher temperatures for thermotectonic processes of granulite formation.

RELATIONSHIP BETWEEN THERMOBAROMETRY, PHASE EQUILIBRIA AND a_{H_2O}

Important first-order constraints on the peak P–T conditions of granulites are provided by a large body of experimental data on the P–T stability of granulite-facies mineral associations (see below). In the absence of low-a_{H_2O} fluid infiltration, the characteristic anhydrous mineralogy of granulites (e.g. Grt, Opx, Cpx, sillimanite) results from supersolidus, vapour-absent dehydration melting reactions that consume muscovite, biotite and/or hornblende and produce a melt phase in addition to the anhydrous minerals (e.g. Brown & Fyfe, 1970; Thompson, 1982). In dehydration melting reactions, a_{H_2O} is *internally controlled* by the melting reaction (Powell, 1983; Clemens & Vielzeuf, 1987; Thompson, 1990) and is therefore a function of the bulk composition (mineral assemblage plus melt) and P–T conditions. Recognizing that a_{H_2O} is a dependent variable in the absence of fluid infiltration provides the justification for evaluating thermobarometry results against the results from experimental fluid-absent phase equilibrium studies.

EXPERIMENTAL CONSTRAINTS ON P–T STABILITY OF GRANULITE-FACIES MINERAL ASSOCIATIONS

Figure 1 shows experimental and thermodynamically predicted positions of reactions that limit the P–T stability of some key granulite-facies mineral assemblages for the three most common bulk compositions, here defined as mafic, intermediate and aluminous. The relevant wet solidi for each composition are also shown. Except at low pressure ($<\sim3$ kbar), the reactions occur above the wet solidi and so are dehydration melting reactions. The dehydration melting reactions shown in Fig. 1 were investigated in vapour-absent experiments, simulating conditions in natural (non-infiltrated) granulites in which any free fluid would have been consumed at the wet solidus down-grade of the dehydration melting reactions. The reaction positions shown in Fig. 1 are for the lowest-temperature occurrence of the diagnostic mineral or mineral association (e.g. Opx), and hence provide lower limits on possible P–T conditions for rocks containing these minerals. To keep the diagrams legible, experimental brackets have been omitted and lines have been drawn by eye approximately through the midpoints of the limiting experiments of the respective studies. At a given pressure, the typical temperature interval between limiting experiments is 25–50°C, so that individual lines should be considered as bands of width ±25°C or so.

Mafic granulites

Mafic granulites (Fig. 1a) are characterized by Cpx- and/or Hbl-bearing Opx + Pl ± Grt ± Bt ± Kfs ± Qtz mineral assemblages, and are broadly basaltic in composition. The general reaction that first introduces Opx to Hbl + Pl ± Qtz ± Cpx ± Grt-bearing mafic amphibolites below ~10 kbar is

$$\text{Hbl} + \text{Qtz} \pm \text{Grt} = \text{Opx} + \text{Cpx} \pm \text{Pl} + \text{L}. \quad (1)$$

At pressures below the solidus, this reaction produces a hydrous vapour phase rather than a melt phase [(1′) in Fig. 1a]. At pressures above ~10 kbar, an analogous reaction introduces Grt + Cpx without Opx:

$$\text{Hbl} + \text{Pl} + \text{Qtz} = \text{Grt} + \text{Cpx} + \text{L} \quad (2)$$

(Pattison, 2003). Quartz-free reactions are also likely, but quartz-bearing reactions are the ones of importance to this study because they occur at lower temperatures (Spear, 1981; Hartel & Pattison, 1996).

Figure 1a shows the experimental constraints on reactions (1) and (2), with reaction (1) being of most interest to this study because it produces Opx. The various experimental studies on reaction (1) are in rather good agreement (850 ± 50°C over the pressure range 3–10 kbar, with no obvious pressure dependence), even though a fairly wide range of starting mineral compositions is represented [see table 1 of Pattison (2003)].

Intermediate granulites

Intermediate granulites (Fig. 1b) are characterized by Cpx- and Hbl-free Opx + Pl ± Grt ± Bt ± Kfs ± Qtz mineral assemblages, and are broadly representative of metamorphosed psammites, semipelites and intermediate–felsic igneous rocks in which the major hydrous mineral is biotite. The general reaction that

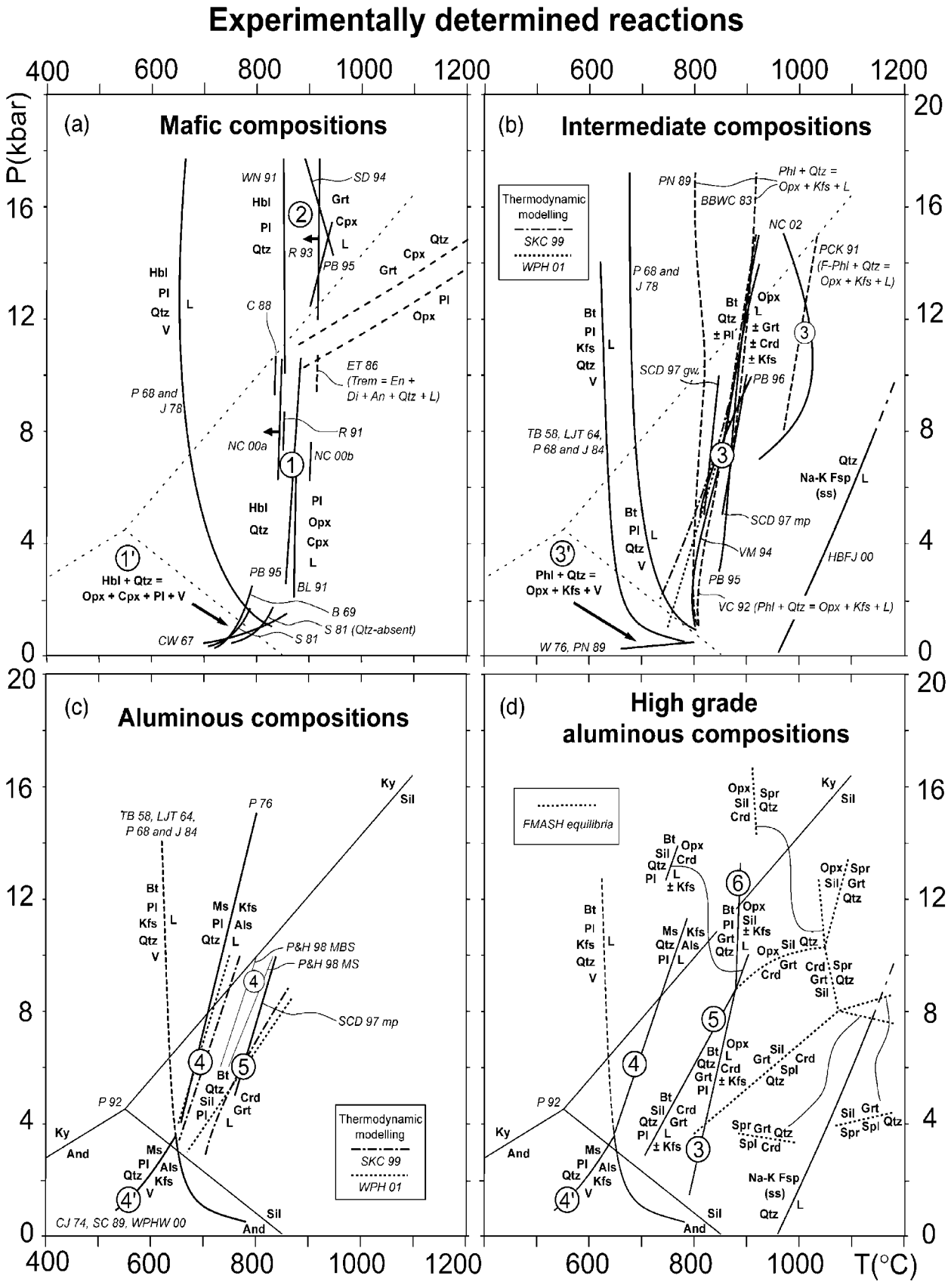
Experimentally determined reactions
(a) Mafic compositions
(b) Intermediate compositions
(c) Aluminous compositions
(d) High grade aluminous compositions
P(kbar)
T(°C)
WN 91
SD 94
R 93
PB 95
C 88
ET 86
(Trem = En + Di + An + Qtz + L)
P 68 and J 78
NC 00a
R 91
NC 00b
BL 91
B 69
S 81 (Qtz-absent)
S 81
CW 67
Hbl + Qtz = Opx + Cpx + Pl + V
PN 89
Phl + Qtz = Opx + Kfs + L
BBWC 83
NC 02
PCK 91 (F-Phl + Qtz = Opx + Kfs + L)
Thermodynamic modelling
SKC 99
WPH 01
SCD 97 gw.
PB 96
TB 58, LJT 64, P 68 and J 84
SCD 97 mp
VM 94
HBFJ 00
Phl + Qtz = Opx + Kfs + V
VC 92 (Phl + Qtz = Opx + Kfs + L)
W 76, PN 89
P 76
P&H 98 MBS
P&H 98 MS
P 92
CJ 74, SC 89, WPHW 00
FMASH equilibria

first introduces Opx to these rocks is

$$\text{Bt} + \text{Qtz} \pm \text{Pl} = \text{Opx} + \text{L} \pm \text{Grt} \pm \text{Crd} \pm \text{Kfs}. \quad (3)$$

At pressures below the solidus, this reaction produces a hydrous vapour phase rather than a melt phase. Figure 1b shows the experimental data on reactions (3) and (3′) in addition to two pertinent wet solidi (one involving K-feldspar and the other not). A wide variety of starting compositions for reaction (3) is represented in Fig. 1b, ranging from end-member phlogopite + quartz to mixtures of different types of natural Bt + Pl + Qtz of widely varying Pl composition and Mg/(Mg + Fe), Ti and F content of biotite. Despite the wide compositional range, most of the experiments fall in an interval ranging from ~800°C at 1 kbar to 900°C at 15 kbar. Vielzeuf & Clemens (1992) discussed the lower temperatures found by Peterson & Newton (1989). The two studies showing the highest-temperature location of reaction (3) (Peterson *et al*., 1991; Nair & Chacko, 2002) used starting biotite compositions containing significant F and/or Ti, such as found in natural biotites from the amphibolite–granulite transition. The two thermodynamically predicted positions of reaction (3) in Fig. 1b (Spear *et al*., 1999; White *et al*., 2001) are calculated for F- and Ti-free biotite. These occur at lower temperature and show a stronger pressure dependence than the experiments.

The position of the reaction curve for dry melting of alkali feldspar solid solution + quartz in the $NaAlSi_3O_8$–$KAlSi_3O_8$–SiO_2 system (Holtz *et al*., 2001) is also shown. The position of this curve is a minimum for natural feldspars because addition of Ca results in an up-temperature displacement (e.g. Johannes, 1978).

Aluminous granulites

Aluminous granulites (Fig. 1c and d) represent metamorphosed pelitic bulk compositions and may contain combinations of the aluminous minerals Grt, Crd, Al_2SiO_5 (sillimanite, kyanite or andalusite), spinel (Spl), sapphirine (Spr), corundum (Crn) and osumilite (Os), in addition to Opx and/or Bt (e.g. Harley, 1989, 1998*a*). Some workers consider any rock with stable Kfs + Al_2SiO_5 to be representative of granulite facies. The first appearance of this association is by the general reaction

$$\text{Ms} + \text{Qtz} \pm \text{Pl} = \text{Al}_2\text{SiO}_5 + \text{L} \pm \text{Kfs} \quad (4)$$

whose position is shown in Fig. 1c. At pressures below the solidus, this reaction [(4′) in Fig. 1c] produces a hydrous vapour phase rather than a melt phase. The experiments of Patiño-Douce & Harris (1998) using natural starting materials place reaction (4) rather higher than the experiments of Pëto (1976) and the thermodynamically modelled positions of Spear *et al*. (1999) and White *et al*. (2001).

Comparing the position of reaction (4) in Fig. 1c with reactions (1) and (3) in Fig. 1a and b, the first appearance of Kfs + Al_2SiO_5 occurs 100–150°C below the first appearance of Opx in mafic and intermediate compositions. In regional and contact metamorphic sequences in which the first development of Kfs + Al_2SiO_5 in metapelites and the first development of Opx in mafic and intermediate composition can both be mapped, the former is invariably significantly down-grade of the latter (e.g. Adirondacks: De Waard, 1969; Bohlen *et al*., 1985; New England: Schumacher *et al*., 1990*a*; Ballachulish: Pattison & Harte, 1991, 1997; East Ontario Grenville, Carmichael in Davidson *et al*., 1990; Broken Hill: Binns, 1964).

We therefore prefer to define the amphibolite–granulite transition in metapelites by mineral associations that develop closer (both spatially in the field and, by extension, in pressure and temperature) to the first appearance of Opx in mafic and intermediate compositions, namely, Grt + Crd + Kfs (at pressures

Fig. 1. (opposite) Experimental and thermodynamically predicted positions of reactions that limit the stability of granulite-facies mineral associations. Numbered reactions are discussed in the text. Reactions (1), (3) and (4) are dehydration melting reactions that occur above the relevant wet solidi, whereas reactions (1′), (3′) and (4′) are the corresponding dehydration reactions that occur below the relevant wet solidi at lower pressure. V, hydrous vapour; L, silicate liquid. Other abbreviations from Kretz (1983). (a) Mafic granulites. B 69, Binns (1969). BL 91, Beard & Lofgren (1991). C 88, Conrad *et al*. (1988). CW 67, Choudhuri & Winkler (1967). ET 86, Ellis & Thompson (1986). J 78, Johannes (1978). NC 00a, Nair & Chacko (2000), Three Valley Gap composition; NC 00b, Nair & Chacko (2000), Kapuskasing composition. P 68, Piwinskii (1968), tonalite 101. PB 95, Patiño-Douce & Beard (1995). R 91, Rushmer (1991). R 93, Rushmer (1993). S 81, Spear (1981). SD 94, Senn & Dunn (1994). WN 91, Winther & Newton (1991). The position of the reaction Grt + Cpx + Qtz = Opx + Pl is dotted in approximately, consistent with thermodynamic modelling. (b) Intermediate granulites. BBWC 83, Bohlen *et al*. (1983*b*). HBFJ 01, Holtz *et al*. (2001); Na–K Fsp (ss) is alkali feldspar solid solution. J 78, Johannes (1978). J 84, Johannes (1984). LJT 64, Luth *et al*. (1964). NC 02, Nair & Chacko (2002). P 68, Piwinskii (1968), granodiorite 102. PB 95, Patiño-Douce & Beard (1995). PB 96, Patiño-Douce & Beard (1996). PN 89, Peterson & Newton (1989). PCK 91, Peterson *et al*. (1991). SCD 97 gw, mp, Stevens *et al*. (1997), greywacke and metapelite compositions. SKC 99, Spear *et al*. (1999). TB 58, Tuttle & Bowen (1958). VC, Vielzeuf & Clemens (1992). VM, Vielzeuf & Montel (1994). W 76, Wood (1976). WPH 01, White *et al*. (2001). The PCK 91 and NC 03 experiments are for biotite compositions enriched in F and/or Ti. (c) Aluminous granulites. CJ 74, Chatterjee & Johannes (1974). J 84, Johannes (1984). LJT 64, Luth *et al*. (1964). P 68, Piwinskii (1968), granite 104. P 76, Pëto (1976). P 92, Pattison (1992). PH 98 ms, mbs, Patiño-Douce & Harris (1998); muscovite schist and muscovite–biotite-schist compositions. SCD 97 mp, Stevens *et al*. (1997), metapelite composition. SKC 99, Spear *et al*. (1999). TB 58, Tuttle & Bowen (1958). WPH 01, White *et al*. (2001). WPHW 00, White *et al*. (2000). (d) High-grade aluminous granulites. Continuous lines, synthesis of results from (b) and (c); dotted lines, high-grade FMASH equilibria from Harley (1998*a*).

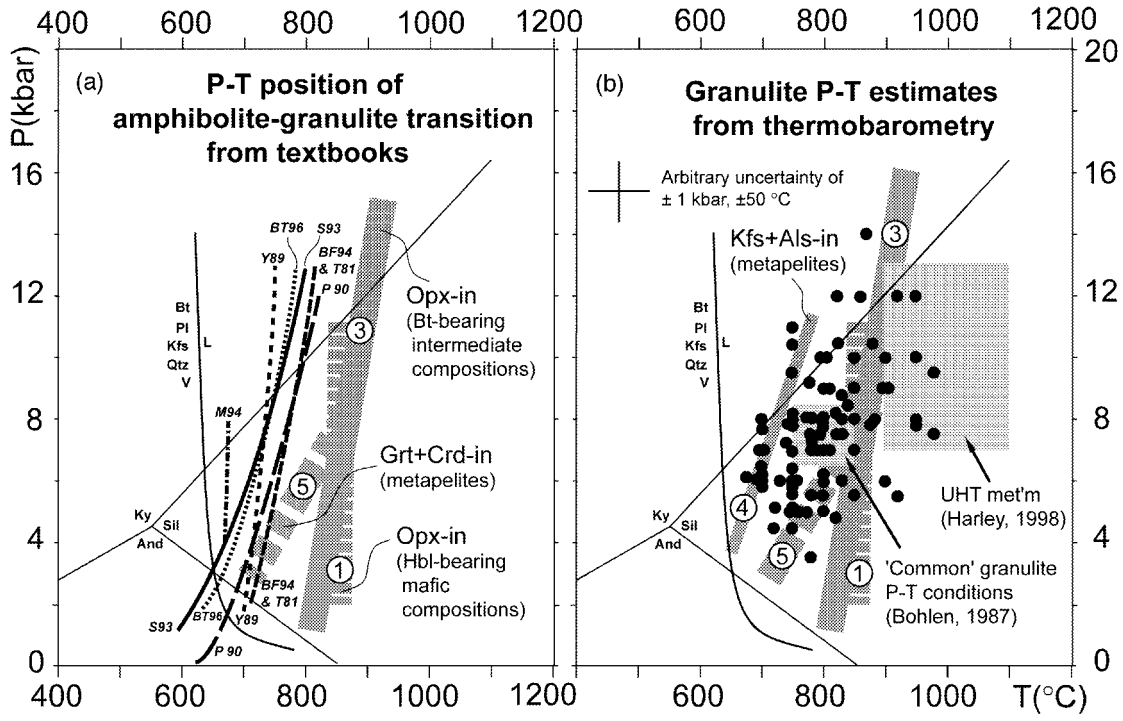

Fig. 2. (a) Location of the amphibolite–granulite transition from current textbooks compared with the granulite facies-limiting reactions from Fig. 1. Reactions are numbered as in the text and Fig. 1. BT, Blatt & Tracy (1996). BF94, Bucher & Frey (1994). M94, Miyashiro (1994). P90, Philpotts (1990). S93, Spear (1993). T81, Turner (1981). Y89, Yardley (1989). (b) Comparison of the granulite facies-limiting reactions from Fig. 1 with the granulite *P–T* estimates from table 1 of Harley (1989), Bohlen's (1987) domain of common granulite *P–T* conditions, and Harley's (1998*a*) domain of ultra-high-temperature metamorphism.

below ~9 kbar) or Opx + Al_2SiO_5 (at pressures above ~9 kbar). The lowest-grade reactions by which these assemblages develop are, respectively,

$$\text{Bt} + \text{Sil} + \text{Qtz} \pm \text{Pl} = \text{Grt} + \text{Crd} + \text{L} \pm \text{Kfs} \quad (5)$$

and

$$\text{Bt} + \text{Grt} + \text{Qtz} \pm \text{Pl} = \text{Opx} + \text{Al}_2\text{SiO}_5 + \text{L} \pm \text{Kfs}. \quad (6)$$

There are only a few experimental data on reaction (5) in Pl-bearing systems (Stevens *et al.*, 1997) (Fig. 1c). Carrington & Harley (1995) provided constraints on reaction (5) in the Pl-free system that formed the basis for the two thermodynamically predicted positions of reaction (5) for Pl-bearing systems in Fig. 1c (Spear *et al.*, 1999; White *et al.*, 2001). The thermodynamically predicted curves are in close agreement but have a shallower slope than indicated by the experiments.

Higher-grade reactions in aluminous granulites involve the minerals or mineral associations sapphirine (Spr), osumilite (Os) and spinel (Spl) + Qtz, with Spr + Qtz indicating particularly high temperatures in excess of 1000°C (e.g. Hensen, 1971; Harley, 1998*a*, 1998*b*). Figure 1d shows the estimated positions of some of the key quartz-bearing reactions in the Fe–Mg–Al_2O_3–SiO_2–H_2O (FMASH) system and their links to reactions (3), (5) and (6). For simplicity, Qtz-absent equilibria and those involving Os have been omitted, even though these are important in a full evaluation of the phase equilibria of 'ultra-high-temperature' metamorphism (Harley, 1998*a*, 1998*b*, and references therein). The positions of most of the high-grade FMASH reactions in Fig. 1d are approximate owing to limited and sometimes conflicting experimental data and the strong effect of the water content of cordierite (Harley, 1998*a*, 1998*b*). In addition, the stability of Spl + Qtz is dependent on Zn content of Spl and on f_{O_2} (Harley, 1998*a*, 1998*b*). Nevertheless, these mineral associations give useful first-order indications of especially high-grade conditions.

Comparison of experimental data with the amphibolite–granulite transition in textbooks and *P–T* estimates from thermobarometry

Figure 2a compares the positions of the granulite-facies-limiting reactions for mafic, intermediate and aluminous compositions [reactions (1), (3) and (5)]

with the amphibolite–granulite boundary from a number of widely used petrology textbooks. The positions of reactions (1), (3) and (5) in Fig. 2 (grey bands) represent the averaged positions from Fig. 1. If the experimental data are accurate simulations of natural granulite-forming reactions, it appears that commonly accepted P–T conditions of the amphibolite–granulite transition are significant underestimates, by $>100°C$. The textbook positions are generally close to reaction (4) (minimum stability of Kfs + Al_2SiO_5; see Fig. 2a), although whether this is just a coincidence is unknown. Most of the textbooks define the amphibolite–granulite transition by the incoming of Opx in common mafic and intermediate bulk compositions, and place the incoming of Al_2SiO_5 + Kfs by reaction (4) in the upper amphibolite facies as discussed above.

Figure 2b compares the position of reactions (1), (3), (4) and (5) with the array of granulite-facies P–T estimates from table 1 of Harley (1989), Bohlen's (1987) P–T box of 'common' granulite P–T conditions, and Harley's (1998*a*, 1998*b*) domain of ultrahigh-temperature metamorphism. Most of the P–T results are derived from conventional thermobarometry. Assigning meaningful uncertainties to the thermobarometry results is virtually impossible owing to the unknown effects of retrograde cation exchange during cooling and the variety of methods used. Arbitrary 'ballpark' uncertainties of ±50°C and ±1 kbar are commonly used (e.g. Harley, 1989). The majority of these P–T estimates fall below the incoming of Opx [reactions (1) and (3)]. Three possibilities to explain this discrepancy are: (1) the experimental data do not accurately simulate the P–T conditions of the reactions in nature, tending to overestimate the minimum conditions required to develop the characteristic granulite-facies mineral associations; (2) the P–T conditions have been generally underestimated; (3) low-a_{H_2O} fluid infiltration is a much more widespread granulite-forming process than previously thought. Accepting the view that fluid infiltration did not occur in most cases, then one of the first two explanations or some combination of them seems most likely. Whereas retrograde cation exchange is perhaps the most obvious possibility, sluggish reaction kinetics of vapour-absent experiments in the crucial temperature range 700–800°C might result in no apparent reaction in experimental run times even when, for the same P–T conditions but at geological time scales, reaction might have proceeded. A few of the experimental studies shown in Fig. 1 addressed this possibility by reversing their experiments (e.g. Peterson & Newton, 1989; Peterson *et al.*, 1991; Vielzeuf & Clemens, 1992; Nair & Chacko, 2002).

GARNET–ORTHOPYROXENE Al-SOLUBILITY BASED THERMOBAROMETRY CORRECTED FOR LATE Fe–Mg EXCHANGE

We attempt to address the above situation by developing and applying a thermobarometry scheme based on Al-solubility in Opx in equilibrium with Grt that corrects for the effects of late Fe–Mg exchange. Al concentrations in Opx are expected to be preserved from peak granulite conditions because of extremely slow diffusion of Al (e.g. Anovitz, 1991) (see data in Table 1).

The rationale and approach of our scheme is not new, having been developed by Fitzsimons & Harley (1994) and Pattison & Bégin (1994*a*), and refined by Chacko *et al.* (1996). The method reported in this paper is largely the same as reported in Chacko *et al.* (1996). Given knowledge of the pressure, the effects of late Fe–Mg exchange are corrected for by adjusting the Fe–Mg ratios of Grt and Opx to bring the Al-solubility and Fe–Mg exchange equilibria involving the two minerals into agreement (i.e. into internal equilibrium). The above workers found that the corrected Al-solubility temperatures were up to 200°C higher than those based on Fe–Mg exchange. We have refined the approach, using more recent thermodynamic data, and applied it to a large number of granulites worldwide to see if the predicted higher temperatures pertain to granulites in general. A key facet of our approach is the evaluation of the thermobarometry results against the limiting P–T conditions of the granulite-facies mineral associations described above. A computer program that performs the calculations, called RCLC (for 'recalculation'), is described below and in Electronic Appendix A. The program and accompanying explanatory notes are available for downloading from the *Journal of Petrology* website at http://www.petrology.oupjournals.org/.or from the authors at http://www.geo.ucalgary.ca/~pattison/drm_pattison-rclc.htm.

Thermodynamic data

Our thermobarometry scheme uses the TWQ2.02b thermodynamic database, based on the thermodynamic data of Berman & Aranovich (1996) with modifications to incorporate the experiments of Aranovich & Berman (1997) on Al-solubility of Opx in equilibrium with Grt in the Fe-end-member system. Use of a single internally consistent database for all phases instead of a range of individually calibrated equilibria (e.g. Harley, 1998*a*, 1998*b*) eliminates problems of inconsistency between calibrations. The Grt–Opx experiments of Lee & Ganguly (1988) were part of the experimental dataset used by Berman & Aranovich

Table 2: Difference between calculated Al-solubility temperatures using TWQ2.02b and experimental temperatures

Study	No. of samples	T(TWQ) – T(exp)	
		Mean	SD
Harley (1984)*	35	−13	38
Lee & Ganguly (1988)	23	−57	90
Nair & Chacko (2002)	6	−35	54

*Experiments in graphite capsules only.

(1996) in the derivation of the thermodynamic data. As a test of the precision and accuracy of the TWQ2.02b database, Grt–Opx Al-solubility temperatures [based on equilibrium (8); see below] were calculated for 64 Grt + Opx-bearing experiments in Fe–Mg ± Ca-bearing systems from three studies (Harley, 1984; Lee & Ganguly, 1988; Nair & Chacko, 2002) (Table 2). Despite the variable quality of some of the experimental Al-solubility data [see discussion in Berman & Aranovich (1996) and Aranovich & Berman (1997)], the mean differences between the calculated temperatures and known experimental temperatures are $<60°C$, and in two of the studies are $<35°C$ (overall mean for 64 samples is $-45°C$). In all cases, the mean calculated temperatures are lower than the mean experimental temperatures, suggesting that TWQ-based P–T results if anything provide slight underestimates.

Thermodynamic system

The thermodynamic system used in RCLC is summarized in Table 3. The rocks of concern contain the Grt + Opx + Pl + Qtz. Eight end-members in the five-component system Ca–Fe–Mg–Al–Si (CFMAS) account for the compositional variability in these phases. The Al-component of Opx is described by the 'orthocorundum' end-member, Al_2O_3 (Aranovich & Berman, 1997), here given the abbreviation 'Al-Op'. Six possible thermodynamic equilibria result, any three of which are independent. The three independent equilibria chosen are:

$$\underset{\text{in Grt}}{Fe_3Al_2Si_3O_{12}} + \underset{\text{in Opx}}{3MgSiO_3} = \underset{\text{in Grt}}{Mg_3Al_2Si_3O_{12}} + \underset{\text{in Opx}}{3FeSiO_3} \quad (7)$$

Table 3: Definition of thermodynamic system for RCLC

Phases:	4	Garnet, Orthopyroxene, Plagioclase, Quartz	
System components:	5	CaO–FeO–MgO–Al_2O_3–SiO_2	
Thermodynamic end-members:	8		
Garnet		Alm	$Fe_3Al_2Si_3O_{12}$
		Prp	$Mg_3Al_2Si_3O_{12}$
		Grs	$Ca_3Al_2Si_3O_{12}$
Orthopyroxene		Fs	$FeSiO_3$
		En	$MgSiO_3$
		Al-Op	Al_2O_3
Plagioclase		An	$CaAl_2Si_2O_8$
Quartz		Qtz	SiO_2
Total number of equilibria:	6		
1 Alm + 3 En = 1 Prp + 3 Fs		(7)	
1 Alm = 3 Fs + 1 Al-Op		(8)	
2 Alm + 1 Grs + 3 Qtz = 6 Fs + 3 An		(9)	
1 Prp = 3 En + 1 Al-Op		(10)	
2 Prp + 1 Grs + 3 Qtz = 6 En + 3 An		(11)	
1 Grs + 2 Al-Op + 3 Qtz = 3 An		(12)	
Number of independent equilibria:	3		

$$\underset{\text{in Grt}}{Fe_3Al_2Si_3O_{12}} = \underset{\text{in Opx}}{3FeSiO_3} + \underset{\text{in Opx}}{Al_2O_3} \quad (8)$$

$$\underset{\text{in Grt}}{2Fe_3Al_2Si_3O_{12}} + \underset{\text{in Grt}}{Ca_3Al_2Si_3O_{12}} + \underset{\text{Qtz}}{3SiO_2} = \underset{\text{in Pl}}{3CaAl_2Si_2O_8} + \underset{\text{in Opx}}{6FeSiO_3} \quad (9)$$

in which Opx is represented by a three-oxygen formula. Equilibria (7) and (8) both involve only Grt and Opx, equilibrium (7) being the Fe–Mg exchange between the two phases and equilibrium (8) being a net-transfer equilibrium controlling the Al-solubility of Opx in equilibrium with Grt. Equilibrium (9) involves all four phases and is the well-known net-transfer barometer in the Fe-end-member system (e.g. Bohlen *et al.*, 1983*b*).

Rationale for Fe–Mg correction

Figure 3 shows two diagrams calculated using the TWQ software (Berman, 1991) for granulite sample PCFM-1 (mineral compositions listed in Table 4). All six equilibria from Table 3 are shown, with the three independent equilibria listed above shown by bold lines. Figure 3a is a typical result for a natural granulite in which the equilibria show considerable scatter, whereas

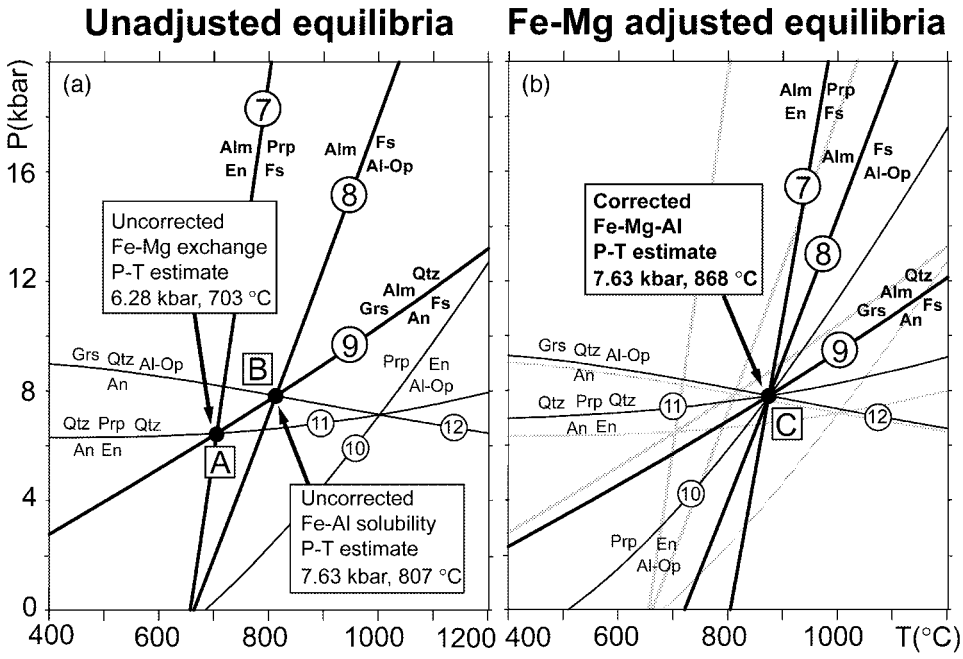

Fig. 3. (a) TWQ plot (Berman, 1991) showing the typical spread in equilibria for a natural Grt + Opx + Pl + Qtz granulite, sample PCFM-1 (mineral composition data in Table 4; modes of Grt:Opx:Bt:Crd = 10:10:0:0). The phases, system components, phase components and equilibria are listed in Table 3. Of the six equilibria shown, only three are independent. The three chosen independent equilibria are indicated in bold. See text for further discussion of equilibria. (b) Same plot as in (a) except that the Fe–Mg ratios of Grt and Opx have been adjusted according to mass-balance constraints so that all equilibria intersect at a point. (See text for further discussion.) The light grey lines are the positions of the curves prior to adjustment.

Table 4: Sample PCFM-1—mineral compositions used for calculations in Fig. 3 and Tables 5 and 6

	Grt	Opx	Crd	Bt	Pl
No. of oxygens:	12	6	18	11	8
Si	3·01	1·90	5·00	2·76	2·69
Ti	0·00	0·01	0·00	0·24	0·00
Al	2·00	0·20	4·00	1·30	1·31
Fe*	1·55	0·66	0·34	0·78	0·00
Mn	0·20	0·01	0·01	0·01	0·00
Mg	1·14	1·23	1·66	1·78	0·00
Ca	0·11	0·00	0·00	0·00	0·31
Na	0·00	0·00	0·00	0·01	0·67
K	0·00	0·00	0·00	0·97	0·02
Total	8·01	4·01	11·01	7·85	5·00

*All Fe assumed to be Fe^{2+}.

Fig. 3b shows the result for the same rock after adjusting the Fe–Mg ratios of the phases as described below.

In Fig. 3a, the intersection of Grt–Opx Fe–Mg exchange equilibrium (7) with the Grt–Opx–Pl–Qtz barometer expression (9) (point A) represents the 'conventional' P–T estimate of the rock (hereafter referred to as the uncorrected Fe–Mg P–T estimate). Aranovich & Berman (1997) advocated use of equilibrium (8), based on Al-solubility in Opx in the Fe-end-member system, as a good method to retrieve peak temperatures because it is relatively robust to late exchange of Fe–Mg. Intersection of equilibrium (8) with equilibrium (9) (point B in Fig. 3a; hereafter referred to as the uncorrected Fe–Al P–T estimate) gives a P–T estimate that is significantly higher than the 'conventional' P–T estimate, consistent with the expected higher closure temperature of Al than of Fe–Mg. However, even this P–T estimate must be in error to some degree because it involves Fe end-members and so must have been affected by the late Fe–Mg exchange. The same comment applies to all of the equilibria in Table 3 and Fig. 3, each of which involves at least one Fe- or Mg-end-member or is affected by Fe–Mg ratio through activity–composition relations.

RCLC corrects for the effects of late Fe–Mg exchange by adjusting the Fe–Mg ratios of the phases according to mass-balance constraints so that all the equilibria intersect at a point (point C in Fig. 3b). This intersection is hereafter referred to as the corrected Fe–Mg–Al P–T estimate. The implicit assumption is that this P–T point represents the condition of equilibrium before the onset of late Fe–Mg exchange (Fitzsimons & Harley, 1994; Pattison & Bégin, 1994*a*). As is the case

with all methods of thermobarometry, this assumption is impossible to prove and may not be correct in all situations (for example, garnet and orthopyroxene may have grown at different times and therefore P–T conditions, or may not have equilibrated with respect to Ca and Al). It nevertheless provides a rationale to correct for the obvious and in some cases substantial effects of late Fe–Mg exchange.

The displacement of each equilibrium for the same amount of Fe–Mg change depends on the standard state free energy (mainly enthalpy) change and the effect of the Fe–Mg change on the equilibrium constant. Whereas equilibria (7), (10) and (11) show substantial displacement (compare Fig. 3a and b), equilibria (8) and (9) show more modest displacement. The corrected Fe–Mg–Al P–T estimate (point C in Fig. 3b) is about 1·4 kbar and 170°C higher than the uncorrected Fe–Mg P–T intersection (point A in Fig. 3a), and about 70°C higher than the uncorrected Fe–Al P–T intersection (point B in Fig. 3a).

Calculation method

To bring the equilibria to convergence, Fe–Mg ratios of Grt and Opx are adjusted according to their modal abundance (assuming to begin with that Grt and Opx are the only two Fe–Mg phases in the rock). Implicit in this approach is that intergranular and intragranular transport of Fe and Mg is efficient enough to effect complete Fe–Mg exchange between the two phases. The sequence of steps to achieve convergence is as follows (refer to Fig. 3):

(1) calculate the P–T position of the intersection of equilibria (8) and (9) (uncorrected Fe–Al P–T estimate; point B in Fig. 3a);
(2) assuming constant bulk-rock composition and using the constraints provided by the modal abundance of Grt and Opx, change their Fe–Mg ratios so that Fe–Mg exchange equilibrium (7) coincides with point B;
(3) recalculate a new position for the intersection of equilibria (8) and (9) using the new Fe–Mg ratios;
(4) repeat several times to obtain convergence.

In rocks that contain Fe–Mg phases in addition to Grt and Opx, such as Crd and Bt, Fe–Mg exchange is assumed to occur amongst all of the phases until Grt and Opx, the slowest Fe–Mg diffusers (Table 1), close to further exchange. Step (2) can therefore be expanded to include Crd and Bt by incorporating their modal abundances into the mass-balance equation, and simultaneously solving for each phases's Fe–Mg ratio so that each of the Grt–Opx, Grt–Bt and Grt–Crd Fe–Mg exchange equilibria coincide with point B.

In the situation that the uncorrected Fe–Mg P–T estimate is higher than the uncorrected Fe–Al P–T estimate (i.e. the positions of points A and B in Fig. 3a are reversed), the correction scheme works in the same way but results in a downward estimate in temperature. This situation probably indicates mineral compositions that are significantly out of equilibrium, perhaps as a result of the effects of retrograde net-transfer reactions, or of closure of one of Grt or Opx to Fe–Mg exchange and continued exchange of the other with Crd and/or Bt as the rock cooled. We can envisage no situation in which Al would exchange to lower temperatures than Fe–Mg. In these situations, the uncorrected Fe–Al P–T estimates are probably more reliable than the corrected Fe–Mg–Al P–T estimates.

Effect of varying mineral modes

Table 5 shows effects of varying mineral modes on the corrected Fe–Mg–Al P–T estimates, using the mineral compositions in Table 4. The effects are rather small, even with extreme variations in modes. Thus, a reasonable P–T estimate can be obtained by performing the convergence technique with Grt and Opx alone, regardless of the other Fe–Mg minerals in the rock. Furthermore, the simplifying assumption that the Fe–Mg adjustment can be taken up wholly by either Grt or Opx introduces relatively little error to the final calculated P–T conditions [see fig. 17 of Pattison & Bégin (1994) for a graphical demonstration of this point]. These considerations become useful if modes or compositional information on Fe–Mg phases in the rock other than Grt and Opx are lacking. On the other hand, the amount by which each phase changes its Fe–Mg ratio varies significantly according to the mode, becoming most extreme for rocks with unequal modal proportions (Table 5).

Sensitivity of the method

Despite the obvious theoretical advantages of Grt–Opx Al-solubility-based thermobarometry, Al concentrations in Opx are typically rather low (1–12 wt % Al_2O_3, mostly in the range 1–5 wt %) and the method is sensitive to small changes in Al concentration. Table 6 shows changes in inferred P–T conditions for different Al concentrations in Opx, with all other mineral compositions held constant and the other elements in Opx varied proportionately (the mineral compositions are those listed in Table 4). For ease of comparison with other studies, X_{Al}^{opx} in Table 6 is the amount of octahedral Al in Opx assuming a six-oxygen formula [rather than the three-oxygen formula used in Table 3 and reactions (7)–(9)]. For uncorrected Fe–Al P–T estimates, the sensitivity increases as the absolute Al concentration drops, going from ~20°C/0·01 X_{Al}^{opx} at $X_{Al}^{opx} = 0{\cdot}13$ (~6 wt %

Table 5: Variation in recalculated temperatures with respect to modal variations for sample PCFM-1 (Table 4)

P–T estimates before correction:	*P* (kbar)	*T* (°C)
Uncorrected Grt–Opx Fe–Mg estimate [intersection of equilibria (7) and (9); point A in Fig. 3a]	6·28	703
Uncorrected Grt–Opx Fe–Al estimate [intersection of equilibria (8) and (9); point B in Fig. 3a]	7·63	807
Intersection of Grt–Bt Fe–Mg exchange and equilibrium (9)	5·81	666
Intersection of Grt–Crd Fe–Mg exchange and equilibrium (9)	6·16	694

Mineral modes				Corrected *P–T*		Changes in Mg/(Mg + Fe)			
Grt	Opx	Crd	Bt	*P* (kbar)	*T* (°C)	ΔGrt	ΔOpx	ΔCrd	ΔBt
10	10	—	—	7·63	868	0·03	−0·02	—	—
10	1	—	—	7·47	881	0·01	−0·05	—	—
1	10	—	—	7·76	857	0·05	0·00	—	—
10	10	10	—	7·69	863	0·04	−0·01	−0·06	—
10	10	—	10	7·72	860	0·04	−0·01	—	−0·04
10	10	10	10	7·76	857	0·05	0·00	−0·05	−0·04
10	1	1	1	7·52	877	0·01	−0·04	−0·09	−0·08
1	10	1	1	7·78	855	0·05	0·00	−0·05	−0·03
1	1	10	1	7·93	841	0·08	0·02	−0·03	−0·01
1	1	1	10	7·90	844	0·07	0·02	−0·03	−0·01

ΔGrt, ΔOpx, ΔCrd, ΔBt: corrected Mg/(Mg + Fe) – initial Mg/(Mg + Fe). Corrected *P–T*: point C in Fig. 3b.

Table 6: Variation in uncorrected Fe–Al and corrected Fe–Mg–Al temperatures as a function of Al concentration in Opx for sample PCFM-1 (Table 4)

X_{Al}	wt % Al_2O_3	Uncorrected Fe–Al		Corrected Fe–Mg–Al	
		P (kbar)	*T* (°C)	*P* (kbar)	*T* (°C)
0·15	6·8	9·6	920	9·7	1050
0·13	5·9	8·9	880	8·9	990
0·11	5·0	8·1	840	8·1	920
0·09	4·1	7·3	790	7·3	840
0·07	3·2	6·4	730	6·4	750
0·05	2·2	5·5	670	5·5	650
0·03	1·3	4·3	570	4·3	480

X_{Al} = Al/2 for six-oxygen Opx. Uncorrected Fe–Al: point B in Fig. 3a. Corrected Fe–Mg–Al: point C in Fig. 3b.

Al_2O_3) to ~50°C/0·01 X_{Al}^{opx} at $X_{Al}^{opx} = 0·03$ (1·3 wt % Al_2O_3). For the corrected Fe–Mg–Al P–T estimates, the effects are stronger (~30°C and 60°C, respectively) because of the magnifying effect of the Fe–Mg correction.

The above considerations show that relatively subtle factors become important to P–T estimation using Grt–Opx Al-solubility methods. These include analytical precision, assumptions about Al partitioning between the tetrahedral and octahedral sites in Opx, and the effects of minor elements such as Na^+, Fe^{3+}, Cr^{3+} and Ti^{4+}.

Droop (1987) and Carson & Powell (1997) discussed strategies for assigning Al between the octahedral and tetrahedral sites of Opx and for determining Fe^{3+} stoichiometrically from microprobe analyses. Regardless of sophistication, no approach can avoid the primary source of error, namely the accuracy and precision of Si and to a lesser degree Fe, Mg and Al. Ignoring initially the issue of Fe^{3+} and other minor elements, calculating X_{Al}^{opx} assuming ideal Tschermak exchange $[(Fe,Mg)^{vi} + Si^{iv} = Al^{vi} + Al^{iv}]$ gives rise to the scheme $X_{Al}^{opx} = Al^{M1} = Al^{total}/2$ (for a six-oxygen Opx formula unit). In our processing of a large body of data from the literature (see below), we have found that this approach results in significantly less scatter and fewer obviously erroneous values than calculating X_{Al}^{opx} by the stricter site occupancy scheme $X_{Al}^{opx} = Al^{M1} = Al^{total} - (2 - Si)$. With regard to Fe^{3+}, in many cases the magnitude of inferred Fe^{3+} is similar to or smaller than the combined analytical uncertainty on Si, Fe, Mg and Al, perhaps accounting for the sometimes unpredictable pattern of calculated Fe^{3+} where there is no independent indication for significant variations in f_{O_2} from oxides or other minerals in the rock. In addition, it is likely that the experimental Opx compositions from which the thermodynamic data were obtained contained at least a small component of Fe^{3+} that is not accounted for (all Fe is assumed to be Fe^{2+}). Unless there is good evidence to indicate otherwise, we are therefore of the opinion that the dangers of overcorrection are as great as the dangers of undercorrection. Nevertheless, RCLC provides a variety of options for estimating X_{Al}^{opx}, including one that takes account of Fe^{3+} and other minor elements.

For the above reasons and in the interests of uniformity (many studies did not analyse for minor elements and/or assumed all Fe was Fe^{2+}), we have followed Fitzsimons & Harley (1994), Aranovich & Berman (1997) and Berman & Bostock (1997) in assuming that $X_{Al}^{opx} = Al/2$ (for a six-oxygen formula). This approach provides a maximum estimate for X_{Al}^{opx}, which in some cases, particularly high-Al metapelites, may result in an overestimate of calculated temperature (see Appendix A and discussion below on Kerala Khondalite Belt). For low concentrations of Al in Opx (e.g. less than ~2 wt % Al_2O_3), such as in many mafic granulites, the accuracy of the Al analysis may become an issue in itself (see discussion below). We therefore encourage reporting the standards used for Opx analysis along with the weight percent oxides.

Scatter in pressure estimates and the use of RCLC-P

Application of RCLC to a few natural datasets results in widely scattered pressure estimates beyond what is reasonable geologically, suggesting that in some samples the analyzed plagioclase and garnet compositions were substantially out of equilibrium. A modified version of RCLC, termed RCLC-P, allows pressure to be input as a known variable and calculates corrected Fe–Mg–Al temperatures by convergence of equilibria (7) and (8) at that pressure [essentially the method of Fitzsimons & Harley (1994) and Pattison & Bégin (1994*a*)]. RCLC-P is also useful if the Grt + Opx-bearing rocks have no plagioclase or the plagioclase compositions were not reported. For example, in estimating the temperatures of the Nain granulites of Berg (1977*a*, 1977*b*), a pressure of 5 kbar was assumed in the absence of information about Pl composition.

Testing of the method

We analyzed three datasets to test the above method. The first is that of Pattison & Bégin (1994*a*), which was concerned with the variation with grain size of the composition of Grt and Opx in two regional granulites from the Minto granulite terrain of northern Quebec. Fe–Mg ratios of core compositions of Grt and Opx show increasing degrees of retrograde exchange as grain size decreases, whereas Al shows little pattern with respect to grain size. Figure 4 shows temperature vs grain size for the uncorrected Fe–Mg, uncorrected Fe–Al and corrected Fe–Mg–Al methods for the two samples. The strong dependence on grain size of the Fe–Mg exchange temperatures is absent from both of the Al-solubility-based methods. In addition, the absolute values of the two Al-solubility methods are in better agreement with the phase equilibrium constraints (estimated from Fig. 1b as 850 ± 25°C at the ~7 kbar pressure of the two samples), with the corrected Fe–Mg–Al temperatures showing the best agreement for B69E.

The second dataset comes from the aureole of the Makhavinekh intrusion, Labrador (McFarlane *et al.*, 2003). In these rocks, regional metamorphic garnet is progressively replaced by Opx + Crd as the contact is approached. Figure 5 shows a profile through the aureole comparing uncorrected Fe–Mg, uncorrected Fe–Al and corrected Fe–Mg–Al temperatures (all assuming a uniform pressure of 5 kbar) as a function of distance from the contact. Whereas the Fe–Mg

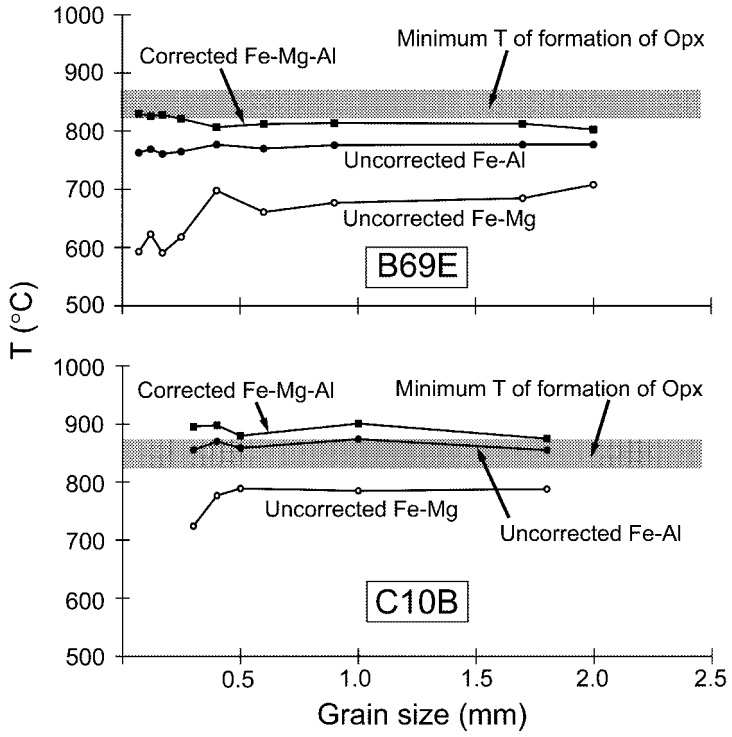

Fig. 4. Plots of temperature vs grain size for two granulites from Pattison & Bégin (1994*a*), using the three methods discussed in the text and shown in Fig. 3. The grain size axis refers to grain size of garnet. The temperatures were calculated using the different garnets and a single Opx grain [see Pattison & Bégin (1994*a*) for further details]. 'Minimum *T* of formation of Opx' is estimated from Fig. 1b for a pressure of 7 kbar, the estimated pressure of formation of the two granulites.

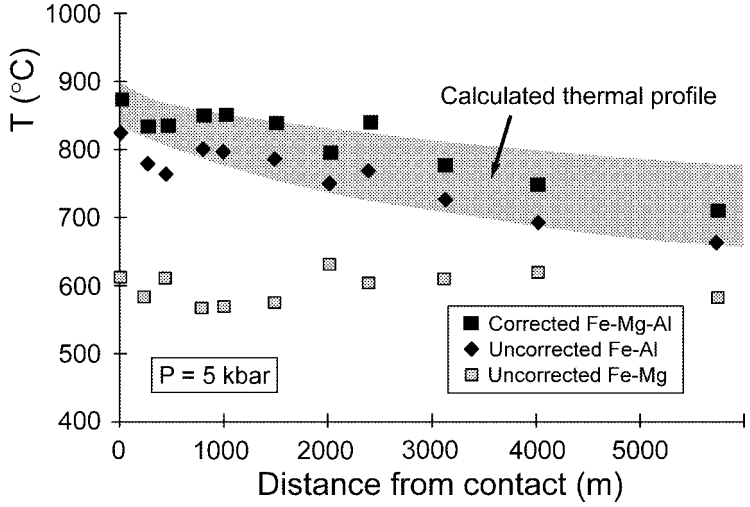

Fig. 5. Makhavinekh aureole, Labrador (McFarlane *et al.*, 2003). Comparison of calculated temperatures with modelled thermal profiles [see McFarlane *et al.* (2003) for details of the modelling]. RCLC-P was used to calculate the temperatures at a fixed pressure of 5 kbar.

exchange temperatures are around 600°C and show no variation within the aureole, the temperatures based on Al-solubility show a pattern of rising temperature as the contact is approached. The Al-solubility-based temperatures fit best with the thermal modelling of McFarlane *et al.* (2003).

The third dataset comes from the ultra-high-temperature rocks of the Napier Complex, Enderby Land, Antarctica (Sheraton *et al.*, 1980). Harley (1985) provided analyses of Grt + Opx-bearing rocks that are interlayered with rocks containing coexisting Spr + Qtz, mesoperthite and metamorphic pigeonite,

together indicative of temperatures above ~1000°C at 8–11 kbar (Harley, 1998*a*, 1998*b*; Fig. 1d). The mean uncorrected Fe–Mg temperature of 750 ± 130°C (error reported as one standard deviation) is a gross underestimate. The uncorrected Fe–Al estimate (880 ± 90°C) is better, whereas the corrected Fe–Mg–Al temperature (950 ± 80°C) is close to the *P–T* conditions indicated by the assemblages.

APPLICATION TO GRANULITES

Based on the success of the three pilot studies, we applied RCLC to 414 Grt + Opx-bearing rocks from 62 granulite terrains using analyses in the literature, and evaluated the results against the phase equilibrium constraints. An obstacle to applying this analysis to more granulite terrains was the relatively common absence of data on the Al content of Opx, particularly in papers written in the 1970s and 1980s, perhaps reflecting the view at that time that Fe–Mg exchange thermometry was all that was needed to estimate peak granulite temperatures. A more subtle factor influencing our results is our lack of control over, and many cases lack of knowledge of, the rationale used in selecting mineral analyses to be used for *P–T* calculations. Different analysis points from the same minerals in the same rock can result in *P–T* estimates that vary by several kilobars in pressure and hundreds of degrees Celsius in temperature (Spear & Florence, 1992; Pattison & Bégin, 1994*a*; Kohn & Spear, 2000). This factor may account for a good deal of the scatter in the results described below.

The Appendix lists the terrains, literature references, sample numbers and type of granulite (mafic, intermediate or aluminous) used in the compilation, the last being based on the mineralogical criteria given earlier. Of the 414 granulite samples examined, 80 are aluminous, 201 are intermediate and 133 are mafic. Electronic Appendix B lists key compositional parameters and calculated *P–T* results for each sample using the uncorrected Fe–Mg, uncorrected Fe–Al and corrected Fe–Mg–Al methods, and is available from the *Journal of Petrology* website or directly from the authors at http://www.geo.ucalgary.ca/~pattison/drm_pattison-research.htm#publications. Table 7 summarizes the results of Electronic Appendix B by listing, for the three types of granulite, the mean, standard deviation, 95% confidence limit on the mean, and range of the compositional parameters and *P–T* estimates. What these statistics actually mean is somewhat unclear, given that the data almost certainly do not represent a Gaussian distribution arising from numerous independent, random perturbations. Systematic perturbations probably cause most of the scatter in the data, most of which result in a lowering of the temperature estimate (see discussion below).

We caution that the results in Table 7 and related figures below show broad trends only and are influenced by the samples and terrains included in the analysis. For example, the ultra-high-temperature Enderby Land terrain and the high-temperature regional contact aureoles around Nain, Labrador, are represented only by intermediate and aluminous samples. In addition, we cannot apply RCLC to Opx-free Grt + Crd-bearing aluminous granulites or to Grt-free Opx+Cpx-bearing mafic granulites. Nevertheless, we believe that our sample base is broad enough that the general trends are meaningful.

Figure 6a and b shows trends of X_{Ca}^{Grt} vs X_{Al}^{opx}, and $Mg/(Mg + Fe)^{opx}$ vs X_{Al}^{opx}, grouped according to type of granulite. Compositional clustering in X_{Ca}^{Grt} vs X_{Al}^{opx} is obvious, with mafic granulites containing the most Ca-rich Grt and Al-poor Opx, aluminous granulites containing the most Ca-poor Grt and Al-rich Opx, and intermediate granulites in between. There is a gap in Grt composition between approximately X_{Ca}^{Grt} of 0·12 and 0·16, with values above the gap largely restricted to mafic mineral assemblages containing either or both of the calcic mafic phases Hbl and Cpx, and values below the gap restricted to intermediate and aluminous mineral assemblages lacking these phases. With respect to $Mg/(Mg + Fe)^{opx}$ vs X_{Al}^{opx}, there is a trend to more Fe-rich compositions in the most Al-poor Opx compositions and a weak trend to higher $Mg/(Mg + Fe)^{opx}$ as Opx becomes more aluminous, similar to that observed experimentally (e.g. Harley, 1984; Lee & Ganguly, 1988).

Figure 7 shows differences in temperature and pressure between the uncorrected Fe–Al and uncorrected Fe–Mg estimates (points B and A in Fig. 3) and between the corrected Fe–Mg–Al and uncorrected Fe–Mg estimates (points C and A in Fig. 3), grouped according to the three compositional types of granulite. Pressure differences between the two sets of estimates are largely the same (Table 7) and so only the difference between corrected Fe–Mg–Al and uncorrected Fe–Mg pressures is displayed. The temperature and pressure differences are strongly correlated because of the dependence of the pressure estimate on the temperature.

Figure 8 illustrates compositional dependence of the results by plotting differences in temperature between the corrected Fe–Mg–Al and uncorrected Fe–Mg estimates against X_{Ca}^{Grt}, X_{Al}^{opx} and $Mg/(Mg + Fe)^{Grt}$, grouped according to type of granulites. Figure 9a plots the mean results from Table 7 with respect to the granulite-facies-limiting reactions from Figs 1 and 2.

Aluminous and intermediate granulites

In aluminous and intermediate granulites, the mean difference between both the uncorrected and corrected Al-solubility-based *P–T* estimates and the uncorrected

Table 7: Compositional parameters and P–T *results for granulites; summary of Electronic Appendix A*

		Aluminous granulites ($n = 80$)				Intermediate granulites ($n = 201$)				Mafic granulites ($n = 133$)			
		Mean	SD	95% CL*	Range	Mean	SD	95% CL*	Range	Mean	SD	95% CL*	Range
Compositional parameters													
X_{Ca}^{Grt}		0·03	0·01	0·002	0·01–0·09	0·06	0·03	0·003	0·01–0·18	0·18	0·02	0·004	0·07–0·25
$Mg/(Mg + Fe)^{Grt}$		0·31	0·13	0·02	0·10–0·58	0·31	0·08	0·01	0·12–0·66	0·27	0·10	0·01	0·03–0·78
$Mg/(Mg + Fe)^{opx}$		0·52	0·13	0·02	0·26–0·76	0·55	0·09	0·01	0·25–0·80	0·53	0·12	0·02	0·10–0·89
X_{Al}^{opx} (= Al/2 for 6-O formula)		0·12	0·04	0·008	0·05–0·22	0·08	0·04	0·005	0·02–0·21	0·04	0·02	0·002	0·01–0·09
P–T *estimates using different methods*													
Uncorrected Fe–Mg	*T* (°C)	732	118	22	475–1156	723	98	11	421–987	793	92	13	518–1034
(point A in Fig. 3a)	*P* (kbar)	5·6	1·9	0·3	2·0–14·1	6·7	1·6	0·2	1·5–11·2	9·6	1·6	0·2	4·8–14·1
Uncorrected Fe–Al	*T* (°C)	854	79	15	672–1059	807	88	10	629–1009	806	70	10	670–982
(point B in Fig. 3a)	*P* (kbar)	6·4	2·2	0·4	3·0–13·5	7·9	1·4	0·2	3·0–12·1	9·8	1·7	0·2	6·5–13·8
Corrected Fe–Mg–Al	*T* (°C)	890	90	17	700–1093	841	98	11	644–1077	816	84	12	656–1081
(point C in Fig. 3b)	*P* (kbar)	6·4	2·2	0·4	3·0–13·5	8·0	1·5	0·2	3·0–12·2	9·9	1·7	0·3	6·6–14·9
P–T *differences between methods*													
Fe–Al − Fe–Mg	*T* (°C)	121	88	16	−138 to 286	84	72	8	−107 to 337	13	75	11	−187 to 195
	P (kbar)	0·8	1·2	0·2	−1·7 to 3·8	1·1	1·0	0·1	−1·5 to 5·3	0·2	1·3	0·2	−3·6 to 3·4
Fe–Mg − Al–Fe–Al	*T* (°C)	45	48	9	−95 to 224	34	35	4	−37 to 177	9	35	5	−81 to 111
	P (kbar)	0·0	0·2	0·04	−1·1 to 0·9	0·1	0·2	0·02	−0·3 to 1·0	0·0	0·1	0·02	−0·3 to 0·5
Fe–Mg − Al–Fe–Mg	*T* (°C)	158	132	24	−233 to 510	118	105	12	−144 to 481	23	109	16	−231 to 292
	P (kbar)	0·9	1·2	0·2	−1·2 to 4·3	1·2	1·1	0·1	−1·4 to 6·3	0·2	1·4	0·2	−3·9 to 4·0

*95% confidence limit on mean = $t \times$ standard error = $t \times$ standard deviation/$\sqrt{n}$, where t is Student's t statistic for 95% confidence interval.

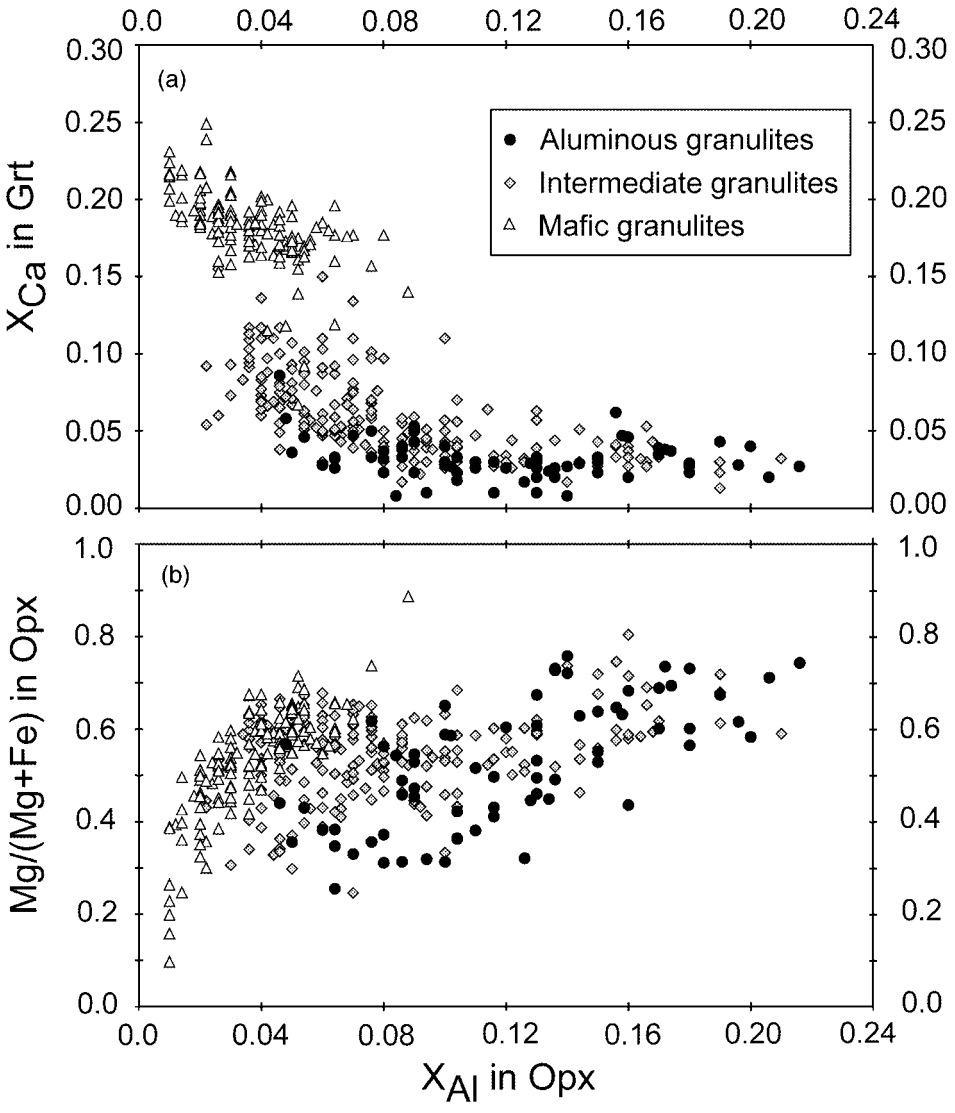

Fig. 6. Mineral composition trends in granulites, grouped by compositional type (aluminous, intermediate, mafic; see text for discussion). (a) X_{Ca}^{Grt} vs X_{Al}^{opx}. $X_{Ca}^{Grt} = Ca/(Ca + Fe + Mn + Mg)$. $X_{Al}^{opx} = Al/2$ for a six-oxygen orthopyroxene formula. (b) $Mg/(Mg + Fe)^{opx}$ vs X_{Al}^{opx}.

Fe–Mg P–T estimates is substantial: 121 ± 16 and 158 ± 24°C, respectively, for aluminous granulites, and 84 ± 8 and 118 ± 12°C, respectively, for intermediate granulites (uncertainties reported as 95% confidence limits on the mean). These values are of a similar magnitude to those found by Fitzsimons & Harley (1994), Pattison & Bégin (1994) and Chacko *et al.* (1996). Pressure differences in both cases are ~1 kbar higher. Regarding absolute temperatures, for aluminous granulites the mean uncorrected Fe–Mg temperature (732 ± 22°C) is substantially below the minimum stability of Opx (Fig. 1), whereas the uncorrected Fe–Al and corrected Fe–Mg–Al temperatures (890 ± 17 and 854 ± 15°C) are consistent with Opx stability (Fig. 9a). The rather high mean corrected Fe–Mg–Al temperature for the aluminous granulites may reflect a combination of sample bias (several samples from ultra-high-temperature localities) and possible temperature overestimation for samples in which there is non-negligible Fe^{3+}. For intermediate granulites, the mean uncorrected Fe–Mg temperature (723 ± 11°C) is substantially below the minimum stability of Opx (Fig. 1), whereas the mean corrected Fe–Mg–Al temperature (841 ± 11°C) satisfies this constraint, with the mean uncorrected Fe–Al temperature (807 ± 10°C) falling in between. We consider that the overall agreement between the Al-solubility-based thermobarometry and the experimental constraints on Opx stability lends support to both approaches, and points to retrograde exchange as the most likely

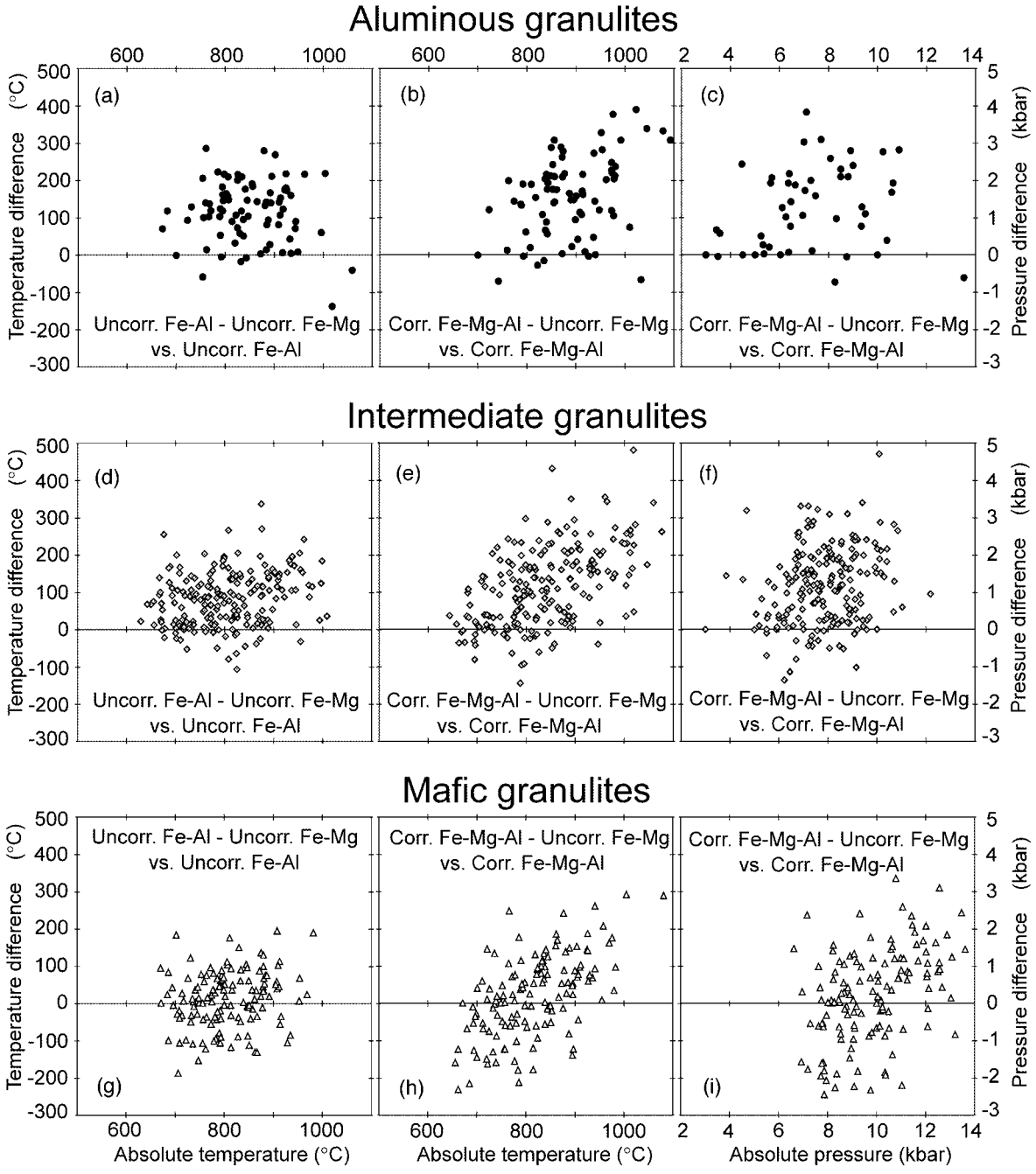

Fig. 7. Temperature or pressure differences between methods vs absolute temperatures or pressures, grouped according to compositional type (aluminous, intermediate, mafic). (a, d, g) Uncorrected Fe–Al temperatures – uncorrected Fe–Mg temperatures. (b, e, h) Corrected Fe–Mg–Al temperatures – uncorrected Fe–Mg temperatures. (c, f, i) Corrected Fe–Mg–Al pressures – uncorrected Fe–Mg pressures. (See text for discussion.)

explanation for the discrepancy between the phase equilibria and geothermobarometry discussed in the Introduction.

We caution that the P–T estimates in Table 7 and Fig. 7 show considerable scatter. This scatter is difficult to attribute to any single factor, arising from some combination of: differences in peak P–T conditions of the samples; varying degrees of retrograde Fe–Mg exchange; retrograde net-transfer reactions; mineral compositions that may not have been in equilibrium before late Fe–Mg exchange; analytical issues relating to the relatively small concentrations of Al in Opx; and

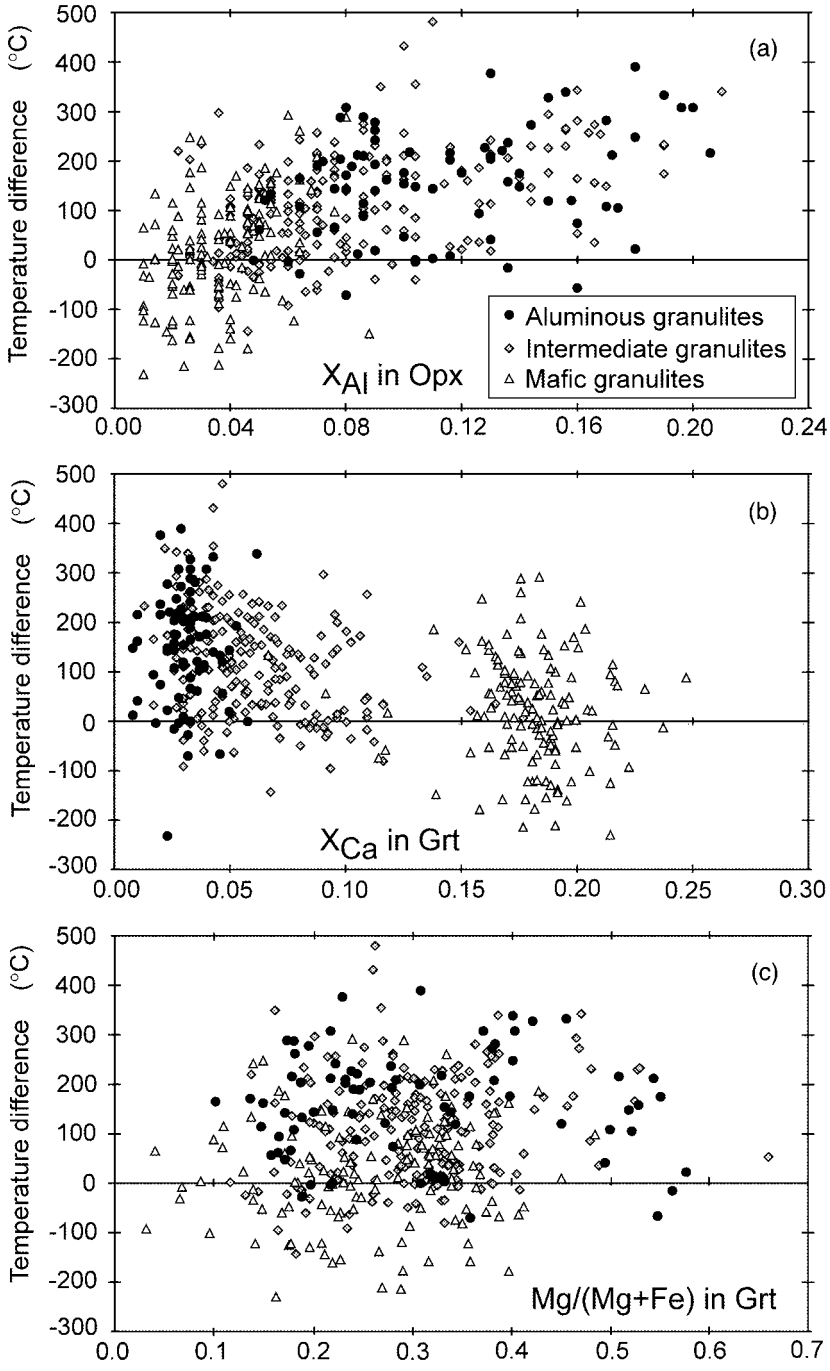

Fig. 8. Temperature differences between corrected Fe–Mg–Al temperatures and uncorrected Fe–Mg temperatures vs mineral compositional parameters, grouped according to compositional type (aluminous, intermediate, mafic). (a) X_{Al}^{opx}. (b) X_{Ca}^{Grt}. (c) $Mg/(Mg + Fe)^{Grt}$. (See caption to Fig. 6 for definition of parameters.)

possible deficiencies in the thermodynamic modelling of Al in Opx, especially at low concentrations (see section below on mafic granulites).

Figure 8a shows that temperature differences between the corrected Fe–Mg–Al and uncorrected Fe–Mg estimates are positively correlated with X_{Al}^{opx}. This correlation is probably due to the fact that, for a given pressure, higher Opx Al contents indicate higher temperatures. The higher the peak temperature is above the closure temperature for Fe–Mg exchange, the greater the expected difference between the calculated Al-solubility and Fe–Mg exchange temperatures.

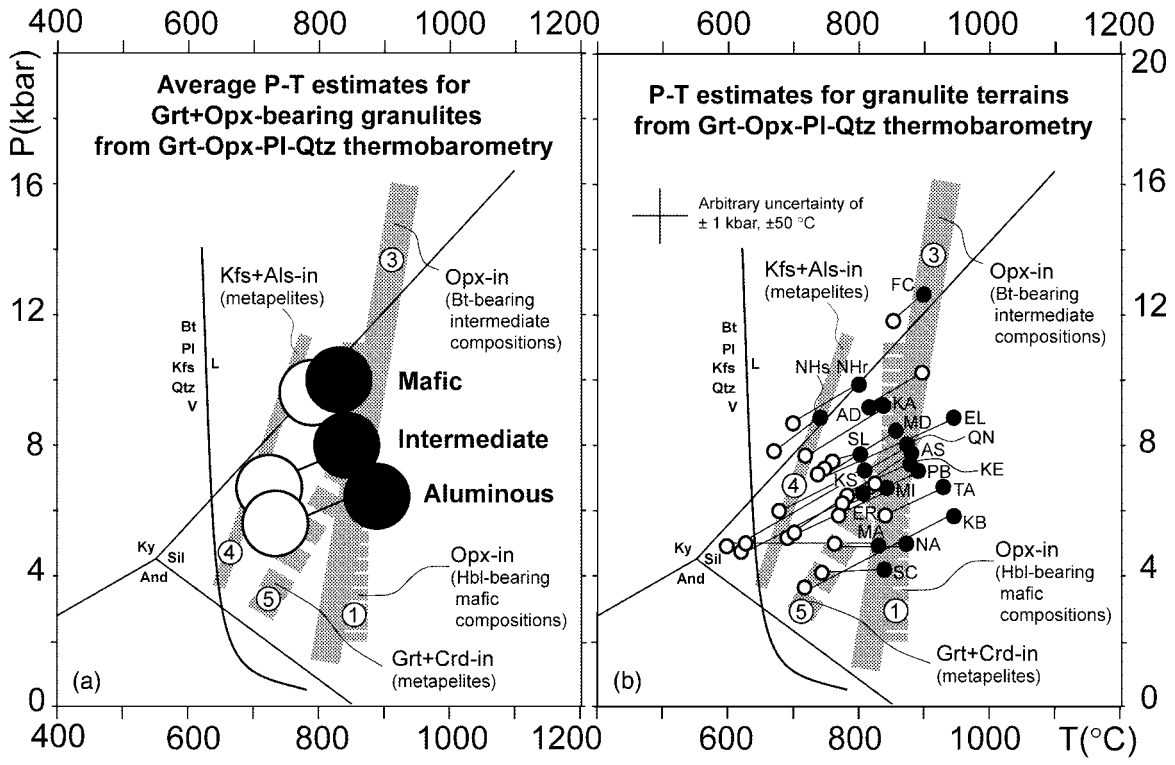

Fig. 9. (a) Comparison of mean P–T results of mafic, intermediate and aluminous granulites containing Grt + Opx with the granulite facies-limiting reactions from Fig. 1. ○, uncorrected Fe–Mg method; ●, corrected Fe–Mg–Al method. Reactions are numbered as in the text and Fig. 1. (b) Comparison of mean P–T results of individual granulite terrains with the limiting granulite facies-limiting reactions from Fig. 1. The label for each terrain is placed beside the corrected Fe–Mg–Al estimate (●). ○, uncorrected Fe–Mg estimates. Abbreviations for the terrains are listed in Table 8. Corrected Fe–Mg–Al temperatures for the three contact metamorphic localities (SC, MA, NA) were calculated for fixed pressure using RCLC-P.

This explanation probably also accounts for the greater spread in corrected Fe–Mg–Al temperatures compared with uncorrected Fe–Al temperatures, especially at higher absolute temperature (compare Fig. 7a and b, and 7d and e, respectively). Figure 8b shows a negative correlation between the above temperature differences and X_{Ca}^{Grt}, probably a secondary effect owing to the fact that X_{Al}^{opx} decreases as X_{Ca}^{Grt} increases (Fig. 6a). Figure 8c shows that there is no significant dependence of temperature difference on $Mg/(Mg + Fe)^{Grt}$.

The mean difference between the corrected Fe–Mg–Al and uncorrected Fe–Al temperatures (points B and C in Fig. 3) is 45 ± 9 and 34 ± 4°C for aluminous and intermediate granulites, respectively (see Table 1). It could be argued that this difference is so small as to be immaterial, supporting Aranovich & Berman's (1997) cautionary view of applying recorrection schemes. Our view is that if demonstrable and systematic errors can be corrected for it is worth while to do so, especially when in a number of cases the difference becomes significant (e.g. Enderby Land examples given above). About 10% of the aluminous and intermediate samples have uncorrected Fe–Mg temperatures that are higher than the uncorrected Fe–Al temperatures. As discussed above, we consider the uncorrected Fe–Al P–T estimates to be more reliable for these samples.

Mafic granulites

In mafic granulites, the mean corrected Fe–Mg–Al estimate (816 ± 12°C) is lower than in the intermediate and aluminous granulites but is still in agreement within error with the phase equilibrium constraints (Fig. 9a). In contrast, the mean uncorrected Fe–Mg exchange estimate (793 ± 13°C) is considerably higher than in the intermediate and aluminous granulites. The higher mean pressure for the mafic granulites (~10 kbar) compared with the intermediate and aluminous granulites (6–8 kbar) is a result of the fact that garnet is a stable phase in mafic granulites only at relatively high pressure (e.g. Pattison, 2003).

The temperature difference between the corrected Fe–Mg–Al estimate and the uncorrected Fe–Mg exchange estimate (23 ± 16°C) is so small as to be insignificant (Table 7). Just under half of the mafic

samples show Fe–Mg temperatures that are higher than Al-solubility-based temperatures (Fig. 7g–i). Figures 6 and 8a and b show that these results correspond to the generally low X_{Al}^{opx} in the more Ca-rich mafic samples.

The reasons for these patterns are unclear. Assuming that Fe–Mg always closes at lower temperature than Al, the most likely explanations are: (1) Fe–Mg diffusion is slower in Ca-rich garnets than in Ca-poor garnets, resulting in a smaller temperature gap between closure of Fe–Mg and Al; (2) the rocks experienced retrograde net-transfer reactions (Spear & Florence, 1992), leading to spuriously high Fe–Mg temperatures; (3) the parts of the Grt and Opx analyzed were not in equilibrium before late Fe–Mg exchange; (4) some of the analytical data for the generally low Al concentrations in Opx in these rocks are in error (too low); (5) the thermodynamic model for Al solubility in Opx loses accuracy at low X_{Al}^{opx}. Although slower Fe–Mg diffusion may account for the higher mean Fe–Mg exchange temperatures, it does not account for the many samples showing Fe–Mg temperatures that are higher than Al-solubility temperatures. Analytical inaccuracy seems unlikely as a general explanation because in studies in which several samples were analyzed using the same procedure (e.g. Adirondack Highlands, Furua Complex: Appendix and Electronic Appendix B), some samples indicate Al-solubility temperatures higher than Fe–Mg temperatures whereas others show the opposite. We see no reason why retrograde net-transfer reactions should be more prevalent in mafic granulites than in aluminous and intermediate granulites. We therefore think that thermodynamic inaccuracy is the most likely single explanation, perhaps augmented in some cases by selection of analysis points on minerals that were not in equilibrium and/or analytical errors. Additional experimental data and attendant thermodynamic modelling bearing on this question are needed.

Comparison with other refractory methods of thermobarometry

The results obtained with our Grt–Opx Al-solubility method are comparable with those obtained with other thermobarometry methods based on refractory cation systems, such as reintegrated feldspar thermometry [Kroll *et al*. (1993) and references therein] and reintegrated Fe–Ti-oxide–olivine–pyroxene thermometry (Frost & Lindsley, 1992; Lindsley & Frost, 1992). For example, reintegrated compositions of mesoperthitic alkali feldspar grains in sample 45-84 from the Kerala Khondalite Belt of south India (Chacko *et al*., 1987) indicate a temperature of 975°C [feldspar model of Fuhrman & Lindsley (1988)] compared with uncorrected Fe–Mg and corrected Fe–Mg–Al temperatures of 821 and 926°C, respectively, for the same sample. Mean corrected Fe–Mg–Al temperatures from the Enderby Land granulites (~950°C; see above) are similar to temperatures calculated from reintegrated mesoperthitic feldspars [950–1050°C, using the analyses of Ellis *et al*. (1980) and Sandiford (1985) and the feldspar model of Fuhrman & Lindsley (1988)], both of which show good agreement with the ultra-high temperatures (>950°C) indicated by metamorphic pigeonite (Sandiford & Powell, 1986) and the Spr + Qtz mineral assemblages. Unfortunately, exsolution features in feldspars and pyroxenes are easily destroyed during later deformation (e.g. Frost & Chacko, 1989), and are therefore considerably less widespread in granulite terrains than Grt–Opx assemblages.

Our results are also comparable with those calculated with the oxygen isotope thermometry method of Farquhar *et al*. (1993), which corrects for the effects of retrograde isotope exchange. In applying this scheme to the high-temperature Enderby Land granulites and Spl + Qtz-bearing Taltson granulites (Chacko *et al*., 1994; Berman & Bostock, 1997; Grover *et al*., 1997), Farquhar *et al*. (1996) retrieved oxygen isotope temperatures >900°C that are consistent with the mineral assemblage stabilities.

Strategies for effective use of the method

The scatter of P–T results using our method calls into question the reliability of any individual P–T estimate, and suggests that to be confident of a P–T estimate for a given area, many samples need to be analyzed. We also advocate element (X-ray) mapping of minerals before analysis points for thermobarometric calculations are selected so that zoning patterns can be interpreted and compositions that are obviously out of equilibrium can be avoided (see Pattison & Bégin, 1994*a*; Kohn & Spear, 2000). Even with X-ray maps, non-central sectioning of Opx grains is an important factor to consider, given the generally small core–rim variation in Al content of individual Opx grains (typically ~1–2 wt %) and the strong temperature dependence on these small changes. An unanswered question of fundamental importance to the use of Al solubility-based thermobarometry is the nature and controls of zoning of Al in Opx (e.g. McFarlane *et al*., 2003).

IMPLICATIONS FOR P–T CONDITIONS OF GRANULITE-FACIES METAMORPHISM

The central conclusion of our study is that a significant number of thermobarometry-based temperature estimates for granulites over the past 30 years are too low

Table 8: P–T results for different terrains

Terrain and abbreviation in Fig. 9		No. of samples	Type	Author(s) estimates		Uncorr. Fe–Mg		Uncorr. Fe–Al		Corr. Fe–Mg–Al	
				T (°C)	*P* (kbar)	*T*	*P*	*T*	*P*	*T*	*P*
Adirondack Highlands	AD	11	M	750–800	7·5–8·0	900	10·2	840	9·2	820	9·2
Ashuanipi	AS	10	I	700–835	3·5–6·5	690	5·2	840	7·3	880	7·8
Enderby Land	EL	25	A	900–950	7·0–10·0	760	7·5	880	8·9	950	8·9
English River	ER	7	I	700–750	5·0	620	4·8	750	6·5	810	6·5
Furua Complex	FC	16	M	800	10·0	850	11·8	890	12·5	900	12·6
Karnataka	KA	7	I/M	700–800	5·0–7·0	720	7·7	800	9·0	840	9·3
Kasai	KS	6	I/A	720	6·7	680	6·0	770	7·2	810	7·2
Kerala Khondalite Belt	KE	34	I/A	700–800	5·0–7·0	780	6·5	880	7·8	920	7·9
Ketilidian Belt	KB	9	A/I	650–800	2·0–4·0	720	3·7	890	5·8	940	5·8
Madras	MD	8	I/M	770–830	6·0–8·0	750	7·4	830	8·4	860	8·5
Makhavinekh	MA	11	A	700–900	5·0	600	5·0	760	5·0	830	5·0
Minto	MI	7	I/A	750–950	6·0–9·0	700	5·3	800	6·7	840	6·7
Nain	NA	16	A	645–915	3·7–6·6	760	5·0	850	5·0	870	5·0
Nilgiri Hills (Srik.)*	NHs	11	I/M	730–750	7·0–10·0	670	7·8	730	8·7	740	8·9
Nilgiri Hills (Raith)†	NHr	51	M/I	730–750	7·0–10·0	700	8·7	760	9·7	800	9·9
Prydz Bay	PB	16	I	860	6·0	780	6·2	860	7·3	890	7·2
Quetico NE	QN	6	I	700	4·0–6·0	630	5·1	810	7·6	880	8·0
Scottish aureoles‡	SC	7	A	700–850	3·0–5·0	740	4·1	830	4·2	840	4·2
Sri Lanka Highlands	SL	10	M/I	820	8·0	740	7·1	780	7·7	800	7·7
Taltson	TA	15	I/A	920–1045	6·0–7·8	840	5·9	910	6·7	930	6·7

Uncorrected Fe–Mg: point A in Fig. 3a. Uncorrected Fe–Al: point B in Fig. 3a. Corrected Fe–Mg–Al: point C in Fig. 3b. M, mafic; I, intermediate; A, aluminous.
*Srikantappa *et al.* (1992) dataset (see Appendix).
†Raith *et al.* (1990) dataset (see Appendix).
‡Combination of Ballachulish and NE Scotland aureoles from Appendix and Electronic Appendix B.
References to localities are given in the Appendix.

and are therefore misleading. Many of these estimates are inconsistent with the stability of the mineral assemblages in the rock. A higher temperature for the amphibolite–granulite transition compared with traditional estimates (Fig. 2a) spreads out the *P–T* range of the upper amphibolite facies. Concomitantly, it reduces the *P–T* interval between 'ordinary' granulite-facies metamorphism and ultra-high-temperature metamorphism (Harley, 1998*a*; Fig. 2b), making the latter the high-temperature end of a continuum rather than a thermally distinct anomaly.

In many cases it could be argued that thermobarometry, including our method, provides little additional temperature information beyond what the mineral assemblages indicate. Where our method of thermobarometry may be most useful is for bulk compositions that maintain the same mineral assemblage over large ranges of elevated *P* and *T*, such as in the 800–1000°C range for intermediate and mafic bulk compositions (e.g. Fig. 1).

P–T ESTIMATES OF GRANULITE TERRAINS

Table 8 provides a summary of mean *P–T* results for 24 terrains with six or more samples. The uncorrected Fe–Mg *P–T* estimates and corrected Fe–Mg–Al *P–T* estimates are plotted in Fig. 9b with respect to the granulite-facies-limiting reactions from Figs 1 and 2. In terrains in which the corrected Fe–Mg–Al *P–T* estimates are lower than the uncorrected Fe–Al *P–T* estimates (e.g. Adirondack Highlands), we have plotted the corrected Fe–Mg–Al *P–T* estimates to maintain consistency, even though we favour the higher estimates.

In some of the terrains, such as the Kerala Khondalite Belt and the Nilgiri Hills, the mean *P–T* estimates are to some degree meaningless because of significant *P–T* variations across the region from which the samples were collected. The main purpose of Fig. 9b is to show that the corrected Fe–Mg–Al *P–T* estimates

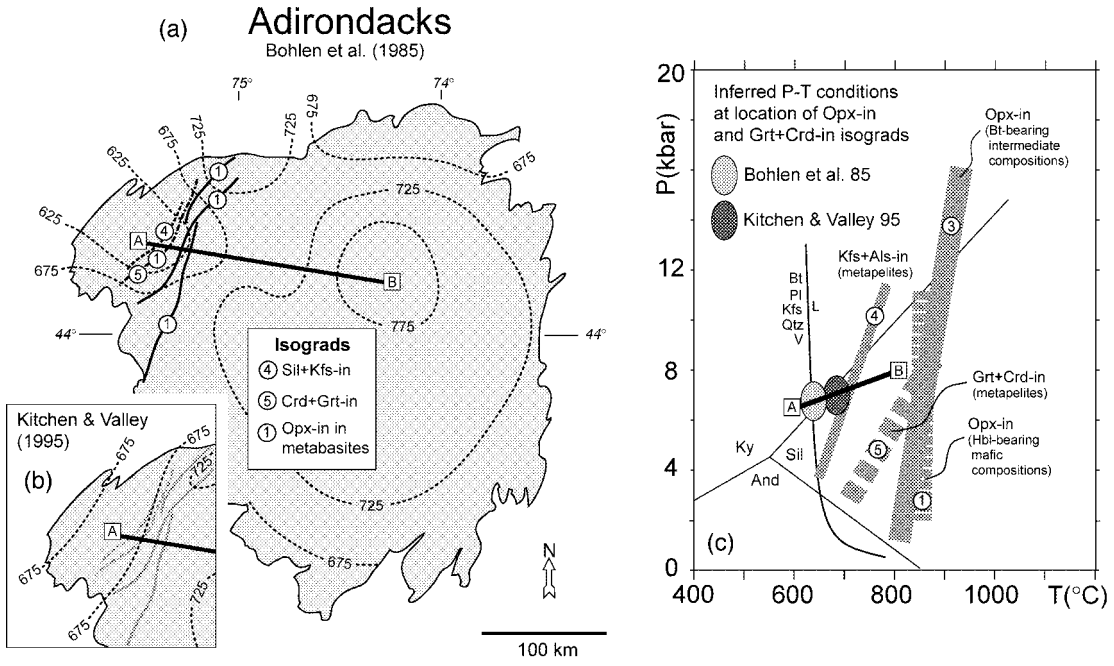

Fig. 10. (a) Map of isograds and metamorphic isotherms in the Adirondacks, from Bohlen *et al.* (1985). The various Opx-in isograds have been discussed by Bohlen *et al.* (1985) and Valley *et al.* (1990). The isograd labelled 1 and 5 represents the close coincidence of the incoming of Opx in metabasites and Crd + Grt in metapelites according to De Waard (1969). (b) Revised isotherms in NW Adirondacks according to Kitchen & Valley (1995). (c) Comparison of P–T conditions along transect A–B in (a) with the granulite facies-limiting reactions and the Kfs + Sil-in reaction from Fig. 1. Reactions are numbered as in the text and Fig. 1. Ovals show the inferred P–T conditions in the vicinity of the Opx-in isograd according to Bohlen *et al.* (1985) and Kitchen & Valley (1995).

largely fall in or close to the granulite-facies stability field, in contrast to the uncorrected Fe–Mg P–T estimates which typically fall well below the granulite-facies stability field. Terrains in which a significant proportion of the sample suite consists of mafic granulites tend to show the lowest P–T estimates [e.g. the Nilgiri Hills datasets of Raith *et al.* (1990) and Srikantappa *et al.* (1992)], and may be unreliable for the reasons discussed above. Some well-known granulite terrains are discussed separately below.

Adirondacks

The Precambrian rocks of the Adirondack region of upper New York State (Fig. 10a) comprise one of the best-known granulite-facies terrains in the world. In their summary papers on the granulite-facies metamorphism of the Adirondacks, Bohlen *et al.* (1985) and Valley *et al.* (1990) presented a pattern of isotherms based on a variety of geothermobarometers that they considered to represent peak or near-peak P–T conditions. Kitchen & Valley (1995) modified the distribution of isotherms in the NW part of the Adirondacks (Fig. 10b). Valley *et al.* (1990) concluded that the granulite-facies metamorphism was largely driven by the magmatic processes of intrusion and partial melting, based on low calculated values of a_{H_2O}, abundance of migmatitic features associated with the granulite mineral assemblages, and absence of evidence for large-scale fluid infiltration.

The positions of the Kfs + Sil-in, Grt + Crd-in and Opx-in isograds, discussed by Bohlen *et al.* (1985), are shown on the map in Fig. 10a. These isograds are represented approximately by reactions (4), (5) and (1), respectively. Figure 10c shows the range of P–T conditions along transect A–B in Fig. 10a compared with the limiting P–T stability fields for Kfs + Sil, Grt + Crd and Opx. The Bohlen *et al.* (1985) P–T conditions are lower by up to 200°C than the minimum stability ranges of Grt + Crd and Opx, and, in the vicinity of the Grt + Crd-in and Opx-in isograds, are below the minimum stability of Kfs + Sil. The somewhat higher temperatures deduced by Kitchen & Valley (1995) are consistent within error of Kfs + Sil stability, but are still considerably lower than those necessary to produce Grt + Crd- or Opx-bearing assemblages.

Three possible explanations are: (1) the peak P–T conditions have been significantly underestimated, especially in the vicinity of the isograds, as a result of retrograde cation exchange from peak conditions; (2) the isotherms record a later cryptic, broadly amphibolite-grade, metamorphic event that reset some element systematics but did not modify the peak mineral

assemblages; (3) low-a_{H_2O} fluid infiltration has been widespread. Locally variable a_{H_2O} in the absence of fluid infiltration is not a tenable explanation if the peak mineral assemblages were developed by partial melting because a_{H_2O} is internally buffered by the mineral + melt assemblage. We accept the evidence of Valley *et al.* (1990) against widespread fluid infiltration and therefore favour an explanation involving P–T underestimation as a result of either retrograde exchange from peak conditions or the effects of a cryptic, lower-grade overprint.

An independent indication of higher peak temperatures in the Adirondack Lowlands in the vicinity of the isograds comes from a recalculated Fe–Mg–Al solubility temperature of 820°C for the one Grt + Opx-bearing sample (RS-34) reported by Edwards & Essene (1988). In the Adirondack Highlands, several recent studies have suggested peak temperatures higher than ~850°C, including those by Spear & Markussen (1997) and Alcock & Muller (1999). A puzzling aspect of the Adirondacks results in Table 8 is the higher mean temperature from Fe–Mg exchange than from the Al-solubility-based methods, which may be due to some or all of the factors discussed above for mafic granulites in general.

Acadian metamorphic high

One of the classic prograde amphibolite–granulite transitions is represented by the Acadian metamorphic high in central Massachusetts. The higher-grade parts consist of the following zones, defined by mineral assemblages in pelitic compositions: Zone III—Ms + Sil zone; Zone IV—Ms + Sil + Kfs zone; Zone V—Kfs + Sil zone; Zone VI—Grt + Crd + Sil + Kfs zone (Schumacher *et al.*, 1990*a*). Within Zone VI, Opx + Cpx + Pl assemblages occur in metabasites. The Zone III–IV transition reaction corresponds approximately to reaction (4), the Zone V–VI transition reaction corresponds approximately to reaction (5), and the development of metabasic Opx + Cpx + Pl assemblages in Zone VI implies P–T conditions above reaction (1). Schumacher *et al.* (1990*a*, fig. 9.9) provided the following approximate temperature boundaries between the zones, based on Grt–Bt Fe–Mg exchange thermometry assuming a pressure of 6 kbar: III–IV, 640°C; IV–V, 670°C; V–VI, 690°C. Thomson (2001) estimated peak temperatures of 700–750°C for Grt + Crd-bearing metapelitic granulites in Zone VI. Whereas Schumacher *et al.*'s Zone III–IV estimate is in reasonable agreement with the minimum stability of Kfs + Sil at 6 kbar (~680°C), the Zone V–VI estimate is >50°C below the minimum stability of Grt + Crd in metapelites [reaction (5)] and >100°C below the minimum stability of Opx + Cpx + Pl in metabasites [reaction (1)] (Fig. 9). Lack of reported Grt + Opx-bearing assemblages in Zone VI does not permit estimation of peak temperatures by our recorrection method.

Incipient charnockites of southern India and Sri Lanka

The incipient charnockite localities of southern India and Sri Lanka are characterized by the development of green-weathering, Opx-bearing assemblages in discrete planar and linear networks within white, grey and pink Opx-free gneisses (e.g. Janardhan *et al.*, 1982). These localities were the focus of intense interest in the 1980s and early 1990s because their formation was ascribed to channelled infiltration of low-a_{H_2O} (carbonic) fluids (e.g. Newton *et al.*, 1980; Janardhan *et al.*, 1982; Hansen *et al.*, 1987; Perchuk *et al.*, 2000), leading to a debate over the relative importance of infiltration-driven carbonic metamorphism vs thermally driven partial melting in the generation of granulites.

We have applied RCLC to 18 incipient charnockite localities in the literature (six of the seven Karnataka–Tamil Nadu samples in the Appendix, eliminating one outlier, and samples 83-123, 4-10a, 121-166, 141-201, M-4, 23, 25, K18-6a, K18-17, 147-214, TN3-1 and TN21-4 from the Kerala Khondalite Belt). Two of the samples are mafic granulites with the rest being intermediate granulites. The mean and 95% confidence limit on the mean of the temperature estimates is 827 ± 18°C for a pressure range of 6–8 kbar, not significantly different from the equivalent values for all intermediate granulites (841 ± 11°C; Table 7). Even though low-a_{H_2O} fluid infiltration appears to have triggered the production of Opx in these localities, the amount by which a_{H_2O} in the fluid was lower than ambient values in the host gneisses might have been rather modest if the host gneisses were close to a temperature where they would produce Opx by closed-system dehydration melting.

This observation supports the suggestion of Frost & Frost (1987) and Clemens (1992) that intrusion and degassing of mafic–charnockitic magmas, partial melting and local low-a_{H_2O} fluid infiltration are expected to be intimately related processes in granulite formation, and may occur in close proximity to one another in individual terrains rather than occurring as terrain-scale end-members. The southern Indian incipient charnockites may therefore represent sporadically developed, slightly lower-temperature, fluid-triggered granulite 'fronts' that develop locally a little downgrade of the main expanse of granulite, the latter controlled largely by magmatic and partial melting processes. A counter-argument to the generality of

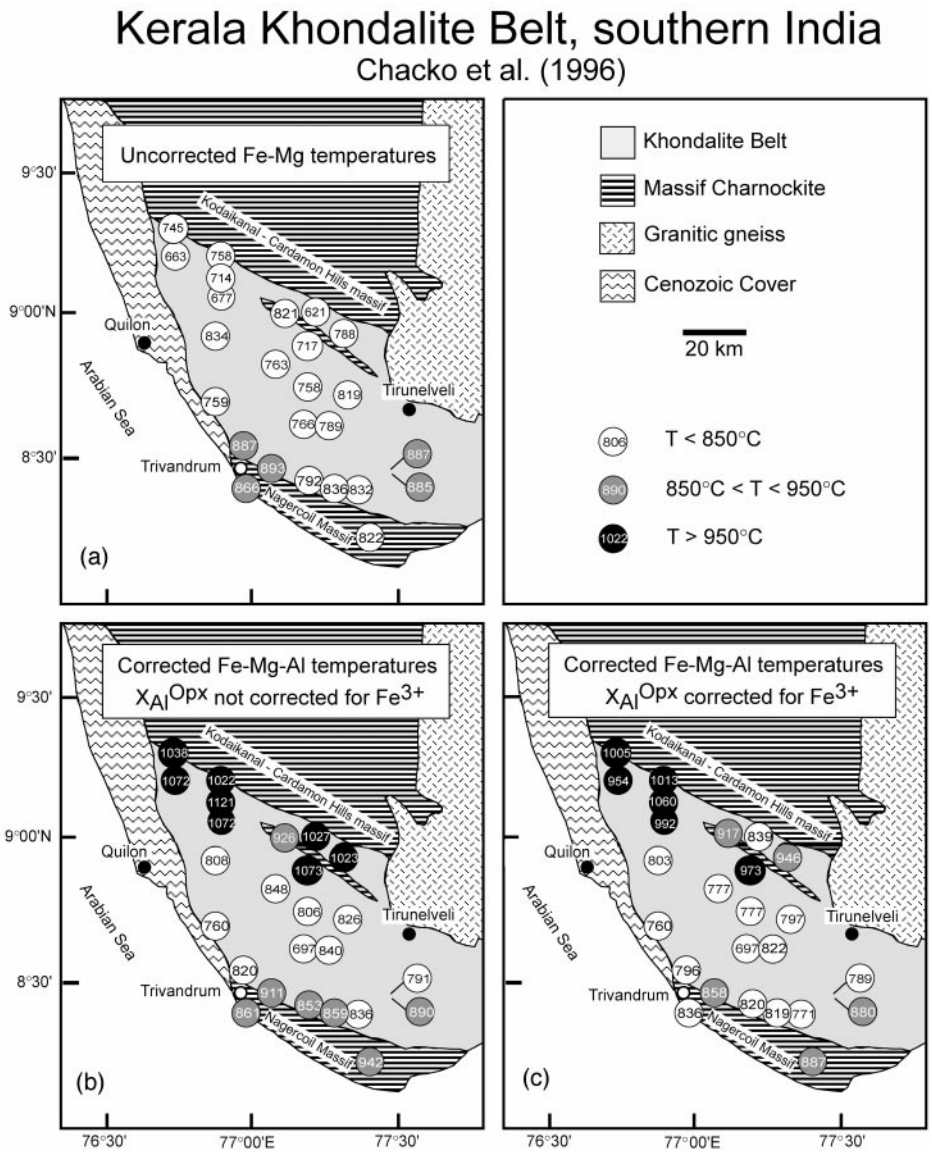

Fig. 11. Generalized geological map of southern India (Chacko *et al*., 1996) showing the dominantly metasedimentary Kerala Khondalite Belt and adjacent Kodaikanal–Cardamon Hills and Nagercoil charnockite massifs. Samples used for thermobarometry have been described by Chacko *et al*. (1996) and are listed in the Appendix and Electronic Appendix B. (a) Uncorrected Grt–Opx Fe–Mg exchange temperatures. Note the absence of any spatial pattern in the temperatures. (b) Corrected Grt–Opx Fe–Mg–Al temperatures. Note the higher temperatures on the margins of the belt adjacent to the charnockite massifs. (c) Corrected Grt–Opx Fe–Mg–Al temperatures taking account of stoichiometrically calculated Fe^{3+} in Opx. Note the somewhat lower temperatures compared with (b) but the same overall regional pattern.

this inference comes from the experimental study by Nair & Chacko (2002) on dehydration melting of the host gneisses to some of the southern India incipient charnockite localities. As is typical of many of the south Indian localities, the gneisses contain biotite with high Ti and F contents. The gneisses did not undergo fluid-absent melting until temperatures in excess of 900°C (at $P \geq 6$ kbar) were reached. For these localities, mean temperatures of ~830°C from RCLC are well below the temperatures necessary for fluid-absent melting, suggesting that a_{H_2O} in the infiltrating fluid was significantly lower than in the host gneisses.

Kerala Khondalite Belt

The Kerala Khondalite Belt (KKB) of southern India (Fig. 11) is an example of a terrain in which the results of Grt–Opx Al-solubility-based P–T estimation resulted in a complete reinterpretation of the P–T

regime and associated thermotectonic evolution (Chacko *et al.*, 1996). Earlier studies based on Fe–Mg exchange methods (e.g. Chacko *et al.*, 1987) suggested a rather uniform P–T regime across the belt of 5–6 kbar and 700–800°C (Fig. 11a). Recalculation of the same samples using RCLC reveals a sharp contrast between a lower P–T (~800–850°C, 6 kbar) central zone with numerous incipient charnockite localities, a northern marginal zone where extreme P–T conditions (>950°C, 9–10 kbar) are found, and a southern marginal zone where less extreme but still elevated temperatures of 850–950°C are found (Fig. 11b). Calculated temperatures taking account of stoichiometrically determined Fe^{3+} in Opx are on average 44°C lower for the whole sample suite but reveal the same regional pattern (Fig. 11c). The elevated temperatures in the marginal zones were attributed by Chacko *et al.* (1996) to the intrusion of igneous charnockite in the massifs to the north and south of the KKB. Nandakumar & Harley (2000) came to similar conclusions based on an independent set of samples.

The >950°C temperatures of the northern zone can be confirmed in a limited number of samples with exsolved feldspars. In the southern zone, Braun *et al.* (1996) found mesoperthites indicating temperatures of 900–1000°C and reported a few occurrences of Spl + Qtz. Interestingly, despite its high temperatures, the northern zone is not characterized by the widespread development of mineral assemblages indicative of ultra-high-temperature conditions (e.g. Spr, Opx + Sil, Spl + Qtz). The paucity of these assemblages may be due to a combination of bulk composition and P–T conditions. The moderate Mg/(Mg + Fe) of most rocks in this region does not favour the formation of the Mg-rich minerals sapphirine or osumulite, and at these relatively high pressures the stability of Spl + Qtz assemblages is restricted to $T > 1000$°C except in oxidized or high-Zn rocks (Fig. 1a). On the other hand, in and adjacent to the Kodaikanal–Cardamon Hills massif, the occurrence of Spr- and Opx + Sil-bearing assemblages (Raith *et al.*, 1997) indicates very high temperatures in the massif as a whole. Thus, in terrains such as the Kerala Khondalite Belt, Grt–Opx thermobarometry may provide the most widely applicable and effective means available for retrieving high-temperature data from granulites that show little mineralogical evidence for such high temperatures.

THERMOTECTONIC MODELLING OF GRANULITES

The indication that most 'ordinary' granulites form at considerably higher temperature than previously assumed carries significant implications for thermotectonic models of granulite formation. In granulites that show isobaric cooling paths and that may have formed along anti-clockwise P–T paths, the heat source for the metamorphism is usually ascribed to mafic magmatic underplating (e.g. Bohlen, 1987; Harley, 1989). In granulites preserving evidence for isothermal decompression and that may have formed along clockwise P–T paths, the metamorphism is commonly ascribed to crustal thickening and associated internal heating in collisional orogens (Bohlen, 1987; Harley, 1989). Using standard mantle heat flow and radioactive heat generation parameters, temperatures in the range 650–800°C can be attained in the middle crust (~20–30 km depth) by this means (England & Thompson, 1984; Patiño-Douce *et al.*, 1990; Ashwal *et al.*, 1992; Jamieson *et al.*, 2002). If, however, mid-crustal granulites typically form at temperatures of ~850°C and above (Fig. 1 and Table 8), much higher heat flow and heat generation parameters, or preferential incorporation of high heat-producing material at mid- to lower-crustal levels (Patiño-Douce *et al.*, 1990; Jamieson *et al.*, 2000) is required. Alternatively, it may be that even in collisional settings, advection of heat into the middle crust by mafic or charnockitic magmas (see Bohlen, 1987; Frost & Frost, 1987; Chacko *et al.*, 1996) may be needed for granulite-facies metamorphism.

ACKNOWLEDGEMENTS

This research was supported by NSERC Discovery Grants 0037233 to D.R.M.P. and 0046751 to T.C. We thank Ron Frost, Simon Harley and Frank Spear for their reviews. D.R.M.P. thanks Jason Krauss, Ron Voordouw and Connie Sullivan for helping to compile data from the literature.

REFERENCES

Ackermand, D., Herd, R. K., Reinhardt, M. & Windley, B. F. (1987). Sapphirine parageneses from the Caraiba complex, Bahia, Brazil: the influence of Fe^{2+}–Fe^{3+} distribution on the stability of sapphirine in natural assemblages. *Journal of Metamorphic Geology* **5**, 323–339.

Alcock, J. & Muller, P. (1999). Very high temperature, moderate pressure metamorphism in the New Russia gneiss complex, northeastern Adirondack Highlands, metamorphic aureole to the Marcy Anorthosite. *Canadian Journal of Earth Sciences* **36**, 1–13.

Anovitz, L. M. (1991). Al-zoning in pyroxene and plagioclase: window on the late prograde to early retrograde P–T paths in granulite terranes. *American Mineralogist* **76**, 1328–1343.

Anovitz, L. M. & Essene, E. J. (1990). Thermobarometry and pressure–temperature paths in the Grenville Province of Ontario. *Journal of Petrology* **31**, 197–241.

Aranovich, L. Ya. & Berman, R. G. (1997). A new garnet–orthopyroxene thermometer based on reversed Al_2O_3 solubility

in $FeO–Al_2O_3–SiO_2$ orthopyroxene. *American Mineralogist* **82**, 345–353.

Arima, M. & Barnett, R. L. (1984). Sapphirine bearing granulites from the Sipiwesk Lake area of the late Archean Pikwitonei granulite terrain, Manitoba, Canada. *Contributions to Mineralogy and Petrology* **88**, 102–112.

Ashwal, L. D., Morgan, P. & Hoisch, T. D. (1992). Tectonics and heat sources for granulite metamorphism of supracrustal-bearing terranes. *Precambrian Research* **55**, 525–538.

Ashworth, J. R. & Chinner, G. A. (1978). Coexisting garnet and cordierite in migmatites from the Scottish Caledonides. *Contributions to Mineralogy and Petrology* **65**, 379–394.

Barth, A. P. & May, D. J. (1992). Mineralogy and pressure–temperature–time path of Cretaceous granulite gneisses, southeastern San Gabriel Mountains, Southern California. *Journal of Metamorphic Geology* **10**, 529–544.

Beard, J. S. & Lofgren, G. E. (1991). Dehydration melting and water-saturated melting of basaltic and andesitic greenstones and amphibolites at 1, 3, and 6·9 kbar. *Journal of Petrology* **32**, 365–401.

Bégin, N. J. & Pattison, D. R. M. (1994). Metamorphic evolution of granulites in the Minto block, northern Québec: extraction of peak P–T conditions taking account of late Fe–Mg exchange. *Journal of Metamorphic Geology* **12**, 411–428.

Berg, J. H. (1977*a*). Dry granulite mineral assemblages in the contact aureoles of the Nain complex, Labrador. *Contributions to Mineralogy and Petrology* **64**, 33–52.

Berg, J. H. (1977*b*). Regional geobarometry in the contact aureoles of the anorthositic Nain complex, Labrador. *Journal of Petrology* **18**, 399–430.

Berman, R. G. (1991). Thermobarometry using multi-equilibrium calculations: a new technique, with petrological applications. *Canadian Mineralogist* **29**, 833–855.

Berman, R. G. & Aranovich, L. Y. (1996). Optimized standard state and mixing properties of minerals: I. Model calibration for olivine, orthopyroxene, cordierite, garnet and ilmenite in the system $FeO–MgO–CaO–Al_2O_3–SiO_2–TiO_2$. *Contributions to Mineralogy and Petrology* **126**, 1–24.

Berman, R. G. & Bostock, H. H. (1997). Metamorphism in the northern Taltson Magmatic Zone, Northwest Territories. *Canadian Mineralogist* **35**, 1069–1091.

Bhattacharya, P. K. & Mukherjee, S. (1987). Granulites in and around the Bengal anorthosite, eastern India; genesis of coronal garnet, and evolution of the granulite–anorthosite complex. *Geological Magazine* **124**, 21–32.

Bingen, B., Demaiffe, D. & Delhal, J. (1988). Aluminous granulites of the Archean Craton of Kasai (Zaire): petrology and P–T conditions. *Journal of Petrology* **29**, 899–919.

Binns, R. A. (1964). Zones of progressive regional metamorphism in the Willyama Complex, Broken Hill district, New South Wales. *Journal of the Geological Society of Australia* **11**, 283–330.

Binns, R. A. (1969). Hydrothermal investigations of the amphibolite–granulite facies boundary. *Special Publication of the Geological Society of Australia* **2**, 341–344.

Blatt, H. & Tracy, R. J. (1996). *Petrology: Igneous, Sedimentary, and Metamorphic*. New York: W. H. Freeman, 529 pp.

Bohlen, S. R. (1987). Pressure–temperature–time paths and a tectonic model for the evolution of granulites. *Journal of Geology* **95**, 617–632.

Bohlen, S. R. & Essene, E. J. (1979). A critical evaluation of two-pyroxene thermometry in Adirondack granulites. *Lithos* **12**, 335–345.

Bohlen, S. R. & Essene, E. J. (1980). Evaluation of coexisting garnet–biotite, garnet–clinopyroxene, and other Mg–Fe exchange thermometers in the Adirondack granulites. *Geological Society of America Bulletin* **91**, 685–719.

Bohlen, S. R., Boettcher, A. L., Wall, V. J. & Clemens, J. D. (1983*a*). Stability of phlogopite–quartz and sanidine–quartz: a model for melting in the lower crust. *Contributions to Mineralogy and Petrology* **83**, 270–277.

Bohlen, S. R., Wall, V. J. & Boettcher, A. L. (1983*b*). Experimental investigation and application of garnet granulite equilibria. *Contributions to Mineralogy and Petrology* **83**, 52–61.

Bohlen, S. R., Valley, J. W. & Essene, E. J. (1985). Metamorphism in the Adirondacks. I. Petrology, pressure and temperature. *Journal of Petrology* **26**, 971–992.

Boullier, A. M. & Barbey, P. (1988). A polycyclic two-stage corona growth in the Iforas Granulitic Unit (Mali). *Journal of Metamorphic Geology* **6**, 235–254.

Bradshaw, J. Y. (1989*a*). Origin and metamorphic history of an Early Cretaceous polybaric granulite terrain, Fiordland, southwest New Zealand. *Contributions to Mineralogy and Petrology* **103**, 346–360.

Bradshaw, J. Y. (1989*b*). Early Cretaceous vein-related garnet granulite in Fiorland, southwest New Zealand: a case for infiltration of mantle-derived CO_2-rich fluids. *Journal of Geology* **97**, 697–717.

Brady, J. B. & McAllister, R. H. (1983). Diffusion data for clinopyroxenes from homogenization and self-diffusion experiments. *American Mineralogist* **68**, 95–105.

Brady, J. B. & Yund, R. A. (1983). Interdiffusion of K and Na in alkali feldspars: homogenization experiments. *American Mineralogist* **68**, 106–111.

Braun, I., Raith, M. & Ravindra Kumar, G. R. (1996). Dehydration melting phenomena in lepynitic gneisses and the generation of leucogranites: a case study from the Kerala Khondalite Belt, southern India. *Journal of Petrology* **37**, 1285–1305.

Brown, G. C. & Fyfe, W. S. (1970). The production of granitic melts during ultrametamorphism. *Contributions to Mineralogy and Petrology* **28**, 310–318.

Bucher, K. & Frey, M. (1994). *Petrogenesis of Metamorphic Rocks*. Berlin: Springer, 320 pp.

Bucher-Nurminen, K. & Ohta, Y. (1993). Granulites and garnet–cordierite gneisses from Dronning Maud Land, Antarctica. *Journal of Metamorphic Geology* **11**, 691–703.

Carrington, D. P. & Harley, S. L. (1995). Partial melting and phase relations in high-grade metapelites: an experimental petrogenetic grid in the KFMASH system. *Contributions to Mineralogy and Petrology* **120**, 270–291.

Carson, C. J. & Powell, R. (1997). Garnet–orthopyroxene geothermometry and geobarometry: error propagation and equilibration effects. *Journal of Metamorphic Geology* **15**, 679–686.

Chacko, T., Kumar, G. R. R. & Newton, R. C. (1987). Metamorphic P–T conditions of the Kerala (south India) Khondalite Belt, a granulite facies supracrustal terrain. *Journal of Geology* **95**, 343–358.

Chacko, T., Creaser, R. A. & Poon, D. (1994). Spinel + quartz granites and associated metasedimentary enclaves from the Taltson Magmatic Zone, Alberta, Canada: a view into the root zone of a high-temperature, S-type granitic batholith. *Mineralogical Magazine* **58a**, 161–162.

Chacko, T., Lamb, M. & Farquhar, J. (1996). Ultra-high temperature metamorphism in the Kerala Khondalite Belt. In: Santosh, M. & Yoshida, M. (eds) *The Archean and Proterozoic Terrains in Southern India within Gondwana*. *Gondwana Research Group Memoir* **3**, 157–165.

Chakraborty, S. & Ganguly, J. (1991). Compositional zoning and cation diffusion in garnets. In: Ganguly, J. (ed.) *Diffusion, Atomic Ordering, and Mass Transport. Advances in Physical Geochemistry* **8**, 120–175.

Chatterjee, N. M. & Johannes, W. (1974). Thermal stability and standard thermodynamic properties of synthetic $2M_1$-muscovite, $KAl_2[AlSi_3O_{10}(OH)_2]$. *Contributions to Mineralogy and Petrology* **48**, 89–114.

Choudhuri, A. & Winkler, H. G. F. (1967). Anthophyllit und Hornblende in einigen metamorphen Reaktionen. *Contributions to Mineralogy and Petrology* **14**, 293–315.

Clemens, J. D. (1992). Partial melting and granulite genesis: a partisan overview. *Precambrian Research* **55**, 297–301.

Clemens, J. D. & Vielzeuf, D. (1987). Constraints on melting and magma production in the crust. *Earth and Planetary Science Letters* **86**, 287–306.

Conrad, W. K., Nicholls, I. A. & Wall, V. J. (1988). Water-saturated and undersaturated melting of metaluminous and peraluminous crustal compositions at 10 kb: evidence for the origin of silicic magmas in the Taupo Volcanic Zone, New Zealand, and other occurrences. *Journal of Petrology* **29**, 765–803.

Coolen, J. J. M. M. M. (1980). *Chemical Petrology of the Furua Granulite Complex, Southern Tanzania. GUA Papers of Geology—Series 1* **13-1980**.

Davidson, A., Carmichael, D. M. & Pattison, D. R. M. (1990). Metamorphism and geodynamics of the Southwestern Grenville Province, Ontario. *International Geological Correlation Program, Projects 235–304: 'Metamorphic Styles in Young and Ancient Orogenic Belts', Field Trip No. 1*. Calgary: University of Calgary, 123 pp.

De Waard, D. (1969). Facies series and P–T conditions of metamorphism in the Adirondack Mountains. *Proceedings, Koninklijke Nederlandse Akademie van Wetenschappen, Series B* **72**, 124–131.

Dempster, T. J., Harrison, T. N., Brown, P. E. & Hutton, D. H. W. (1991). Low-pressure granulites from the Ketilidian Mobile Belt of southern Greenland. *Journal of Petrology* **32**, 979–1004.

Dowty, E. (1980). Crystal-chemical factors affecting the mobility of ions in minerals. *American Mineralogist* **65**, 174–182.

Droop, G. T. R. (1987). A general equation for estimating Fe^{3+} concentrations in ferromagnesian silicates and oxides from microprobe analyses, using stoichiometric criteria. *Mineralogical Magazine* **51**, 431–435.

Droop, G. T. R. & Charnley, N. R. (1985). Comparative geobarometry of pelitic hornfelses associated with the Newer gabbros: a preliminary study. *Journal of the Geological Society, London* **142**, 53–62.

Edwards, R. L. & Essene, E. J. (1988). Pressure, temperature and C–O–H fluid fugacities across the amphibolite–granulite transition, northwest Adirondack Mountains, New York. *Journal of Petrology* **29**, 39–72.

Ellis, D. J. & Thompson, A. B. (1986). Subsolidus and partial melting reactions in the quartz-excess $CaO + MgO + Al_2O_3 + SiO_2 + H_2O$ system under water-excess and water-deficient conditions to 10 kb: some implications for the origin of peraluminous melts from mafic rocks. *Journal of Petrology* **27**, 91–121.

Ellis, D. J., Sheraton, J. W., England, R. N. & Dallwitz, W. B. (1980). Osumilite–sapphirine–quartz granulites from Enderby Land, Antarctica—mineral assemblages and reactions. *Contributions to Mineralogy and Petrology* **72**, 123–143.

England, P. C. & Thompson, A. B. (1984). Pressure–temperature–time paths of regional metamorphism. I. Heat transfer during the evolution of regions of thickened continental crust. *Journal of Petrology* **25**, 894–928.

Farquhar, J., Chacko, T. & Frost, B. R. (1993). Strategies for high-temperature oxygen isotope thermometry: a worked example from the Laramie Anorthosite Complex, Wyoming, USA. *Earth and Planetary Science Letters* **117**, 407–422.

Farquhar, J., Chacko, T. & Ellis, D. J. (1996). Preservation of oxygen isotope compositions in granulites from Northwestern Canada and Enderby Land, Antarctica: implications for high-temperature isotopic thermometry. *Contributions to Mineralogy and Petrology* **123**, 213–224.

Fitzsimons, I. C. W. & Harley, S. L. (1994). The influence of retrograde cation exchange on granulite P–T estimates and a convergence technique for the recovery of peak metamorphic conditions. *Journal of Petrology* **35**, 543–576.

Foland, K. A. (1974) Alkali diffusion in orthoclase. *In*: Hofmann, A. W., Giletti, B. J., Yoder, H. S. & Yund, R. A. (eds.) *Geochemical Transport and Kinetics. Carnegie Institute of Washington Publication* **634**, 77–98.

Frost, B. R. & Chacko, T. (1989). The granulite uncertainty principle: limitations on thermobarometry in granulites. *Journal of Geology* **97**, 435–450.

Frost, B. R. & Frost, C. D. (1987). CO_2, melts, and granulite metamorphism. *Nature* **327**, 503–506.

Frost, B. R. & Lindsley, D. H. (1992). Equilibria among Fe–Ti oxides, pyroxenes, olivine, and quartz: Part II application. *American Mineralogist* **77**, 1004–1020.

Fuhrman, M. L. & Lindsley, D. H. (1988). Ternary-feldspar modeling amd thermometry. *American Mineralogist* **73**, 201–215.

Ganguly, J. & Tazzoli, V. (1994). Fe^{2+}–Mg interdiffusion in orthopyroxene: retrieval from the data on intracrystallization exchange reaction. *American Mineralogist* **79**, 930–937.

Ganguly, J. & Tirone, M. (1999). Diffusion closure temperature and age of a mineral with arbitrary extent of diffusion: theoretical formulation and applications. *Earth and Planetary Science Letters* **170**, 131–140.

Glassley, W. E. & Sorensen, K. (1980). Constant P_s–T amphibolite to granulite facies transition in Agto (West Greenland) metadolerites: implications and applications. *Journal of Petrology* **21**, 69–105.

Grant, J. A. & Frost, B. R. (1990). Contact metamorphism and partial melting of pelitic rocks in the aureole of the Laramie anorthosite complex, Morton Pass, Wyoming. *American Journal of Science* **290**, 425–427.

Grew, E. S. (1981). Granulite-facies metamorphism at Molodezhanaya Station, East Antarctica. *Journal of Petrology* **22**, 297–336.

Griffin, W. L., McGregor, V. R., Nutman, A., Taylor, P. N. & Bridgwater, D. (1980). Early Archaean granulite-facies metamorphism south of Ameralik, West Greenland. *Earth and Planetary Science Letters* **50**, 59–74.

Grove, T. L., Baker, M. B. & Kinzler, R. J. (1984). Coupled CaAl–NaSi diffusion in plagioclase feldspar: experiments and applications to cooling rate speedometry. *Geochimica et Cosmochimica Acta* **48**, 2113–2121.

Grover, T. W., Pattison, D. R. M., MacNicol, V. J. & McDonough, M. J. (1997). Thermotectonic evolution of the Taltson belt and associated shear zones, NE Alberta. *Canadian Mineralogist* **35**, 1051–1067.

Hand, M., Scrimgeour, I., Powell, R., Stuwe, K. & Wilson, C. J. L. (1994). Metapelitic granulites from Jetty Peninsula, east Antarctica: formation during a single event or by polymetamorphism? *Journal of Metamorphic Geology* **12**, 557–573.

Hansen, E. & Stuk, M. (1993). Orthopyroxene-bearing mafic migmatites at Cone Peak, California: evidence for the formation of migmatitic granulites by anatexis in an open system. *Journal of Metamorphic Geology* **11**, 291–307.

Hansen, E. C., Janardhan, A. S., Newton, R. C., Prame, W. K. B. N. & Kumar, G. R. R. (1987). Arrested charnockite formation in southern India and Sri Lanka. *Contributions to Mineralogy and Petrology* **96**, 225–244.

Harley, S. L. (1984). The solubility of alumina in orthopyroxene coexisting with garnet in FeO–MgO–Al_2O_3–SiO_2 and CaO–FeO–MgO–Al_2O_3–SiO_2. *Journal of Petrology* **25**, 665–696.

Harley, S. L. (1985). Garnet–orthopyroxene bearing granulites from Enderby Land, Antarctica: metamorphic pressure–temperature–time evolution of the Archaean Napier Complex. *Journal of Petrology* **26**, 819–856.

Harley, S. L. (1989). The origins of granulites: a metamorphic perspective. *Geological Magazine* **126**, 215–247.

Harley, S. L. (1998*a*). On the occurrence and the characterization of ultrahigh-temperature crustal metamorphism. In: Treloar, P. J. & O'Brien, P. J. (eds) *What Drives Metamorphism and Metamorphic Reactions? Geological Society, London, Special Publication* **138**, 81–107.

Harley, S. L. (1998*b*). An appraisal of peak temperatures and thermal histories in ultrahigh-temperature (UHT) crustal metamorphism: the significance of aluminous orthopyroxene. *Memoirs of National Institute of Polar Research, Special Issue* **53**, 49–73.

Harley, S. L. & Fitzsimons, I. C. W. (1991). Pressure–temperature evolution of metapelitic granulites in a polymetamorphic terrane: the Rauer Group, East Antarctica. *Journal of Metamorphic Geology* **9**, 231–243.

Harley, S. L., Hensen, B. J. & Sheraton, J. W. (1990). Two-stage decompression in orthopyroxene–sillimanite granulites from Forefinger Point, Enderby Land, Antarctica: implications for the evolution of the Archaean Napier Complex. *Journal of Metamorphic Geology* **8**, 591–613.

Harris, N. W. B., Holt, R. W. & Drury, S. A. (1982). Geobarometry, geothermometry and late Archean geotherms from the granulite facies terrain of south India. *Journal of Geology* **90**, 509–527.

Hartel, T. H. D. & Pattison, D. R. M. (1996). Genesis of the Kapuskasing (Ontario) migmatitic mafic granulites by dehydration melting of amphibolite: the importance of quartz to reaction progress. *Journal of Metamorphic Geology* **14**, 591–611.

Hensen, B. J. (1971). Theoretical phase relations involving cordierite and garnet in the system MgO–FeO–Al_2O_3–SiO_2. *Contributions to Mineralogy and Petrology* **33**, 191–214.

Holtz, F., Becker, A., Freise, M. & Johannes, W. (2001). The water-undersaturated and dry Qz–Ab–Or system revisited. Experimental results at very low water activities and geological implications. *Contributions to Mineralogy and Petrology* **141**, 347–357.

Iyer, S. S., Choudhuri, A., Pattison, D. R. M. & De Paoli, G. R. (1996). Petrology and geochemistry of the Neoproterozoic Guaxupé granulite facies terrain, southeastern Brazil. *Precambrian Research* **77**, 23–40.

Jamieson, R. A., Beaumont, C., Vanderhaeghe, O. & Fullsack, P. (2000). How does the lower crust get hot? *Geological Association of Canada–Mineralogical Association of Canada Annual Meeting, Abstracts with Program*, 497.

Jamieson, R. A., Beaumont, C., Nguyen, M. H. & Lee, B. (2002). Interaction of metamorphism, deformation, and exhumation in large convergent orogens. *Journal of Metamorphic Geology* **20**, 9–24.

Janardhan, A. S., Newton, R. C. & Hansen, E. C. (1982). The transformation of amphibolite facies gneiss to charnockite in southern Karnataka and northern Tamil Nadu, India. *Contributions to Mineralogy and Petrology* **79**, 130–149.

Jaoul, O., Sautter, V. & Abel, F. (1991). Nuclear microanalysis: a powerful tool for measuring low atomic diffusivity with mineralogical applications. In: Ganguly, J. (ed.) *Diffusion, Atomic Ordering and Mass Transport. Advances in Physical Geochemistry* **8**, 198–220.

Johannes, W. (1978). Melting of plagioclase in the system Ab–An–H_2O and Qz–Ab–An–H_2O at $PH_2O = 5$ kbar, an equilibrium problem. *Contributions to Mineralogy and Petrology* **66**, 295–303.

Johannes, W. (1984). Beginning of melting in the granite system Qz–Or–Ab–An–H_2O. *Contributions to Mineralogy and Petrology* **86**, 264–273.

Johansson, L., Lindh, A. & Möller, C. (1991). Late Sveconorwegian (Grenville) high pressure granulite facies metamorphism in southwest Sweden. *Journal of Metamorphic Geology* **9**, 283–292.

Kitchen, N. E. & Valley, J. W. (1995). Carbon isotope thermometry in marbles of the Adirondack Mountains, New York. *Journal of Metamorphic Geology* **13**, 577–594.

Kohn, M. J. & Spear, F. S. (2000). Retrograde net transfer reaction insurance for pressure–temperature estimates. *Geology* **28**, 1127–1130.

Komatsu, M., Toyoshima, T., Osanai, Y. & Arai, M. (1994). Prograde and anatectic reactions in deep arc crust exposed in the Hidaka metamorphic belt, Hokkaido, Japan. *Lithos* **33**, 31–49.

Kretz, R. (1983). Symbols for rock-forming minerals. *American Mineralogist* **68**, 277–279.

Kroll, H., Evangelakakis, C. & Voll, G. (1993). Two feldspar geothermometry: a review and revision for slowly cooled rocks. *Contributions to Mineralogy and Petrology* **114**, 510–518.

Lal, R. K., Ackermand, D. & Upadhyay, H. (1987). *P–T–X* relationships deduced from corona textures in sapphirine–spinel–quartz assemblages from Paderu, Southern India. *Journal of Petrology* **28**, 1139–1168.

Lamb, R. C., Smalley, P. C. & Field, D. (1986). *P–T* conditions for the Arendal granulites, southern Norway: implications for the roles of *P*, *T* and CO_2 in deep crustal LILE-depletion. *Journal of Metamorphic Geology* **4**, 143–160.

Lasaga, A. C. (1983). Geospeedometry: an extension of geothermometry. In: Saxena, S. K. (ed.) *Kinetics and Equilibrium in Mineral Reactions. Advances in Physical Geochemistry* **3**, 81–114.

Lasaga, A. C., Richardson, S. M. & Holland, H. D. (1977). The mathematics of cation diffusion and exchange between silicate minerals during retrograde metamorphism. In: Saxena, S. K. & Bhattacharji, S. (eds) *Energetics of Geological Process*. New York: Springer, pp. 353–388.

Lee, H. Y. & Ganguly, J. (1988). Equilibrium compositions of coexisting garnet and orthopyroxene: experimental determinations in the system FeO–MgO–Al_2O_3–SiO_2, and applications. *Journal of Petrology* **29**, 93–113.

Lindsley, D. H. & Frost, B. R. (1992). Equilibria among Fe–Ti oxides, pyroxenes, olivine, and quartz: Part I. Theory. *American Mineralogist* **77**, 987–1003.

Loock, G., Stosch, H. G. & Seck, H. A. (1990). Granulite facies lower crustal xenoliths from the Eifel, West Germany: petrological and geochemical aspects. *Contributions to Mineralogy and Petrology* **105**, 25–41.

Luth, W. C., Jahns, R. H. & Tuttle, O. F. (1964). The granite system at pressures of 4 to 10 kbars. *Journal of Geophysical Research* **69**, 759–773.

McFarlane, C. R. M., Carlson, W. D. & Connelly, J. N. (2003). Prograde, peak, and retrograde *P–T* paths from aluminum in orthopyroxene: high-temperature contact metamorphism in the aureole of the Nain Plutonic Suite. *Journal of Metamorphic Geology* in press.

Mengel, F. & Rivers, T. (1991). Decompression reactions and *P–T* conditions in high-grade rocks, Northern Labrador: *P–T–t* paths

from individual samples and implications for Early Proterozoic tectonic evolution. *Journal of Petrology* **32**, 139–167.

Mengel, F. & Rivers, T. (1997). Metamorphism in the Paleoproterozoic Torngat orogen, Labrador: petrology and P–T–t paths of amphibolite- and granulite-facies rocks across Komaktorvik shear zone. *Canadian Mineralogist* **35**, 1137–1160.

Miyashiro, A. (1994). *Metamorphic Petrology*. New York: Oxford University Press, 404 pp.

Mohan, A. & Windley, B. F. (1993). Crustal trajectory of sapphire-bearing granulites from Ganguvarpatti, South India: evidence for an isothermal decompression path. *Journal of Metamorphic Geology* **11**, 867–878.

Munyanyiwa, H., Touret, J. L. R. & Jelsma, H. A. (1993). Thermobarometry and fluid evolution of enderbites within the Magondi Mobile Belt, Northern Zimbabwe. *Lithos* **29**, 163–176.

Nair, R. & Chacko, T. (2000). Fluid-absent melting of two high grade amphibolites: constraints on the conditions required for orthopyroxene formation. *Geological Association of Canada–Mineralogical Association of Canada Annual Meeting, Abstracts with Program* **24**, 2121–2042.

Nair, R. & Chacko, T. (2002). Fluid-absent melting of high-grade semi-pelites: P–T constraints on orthopyroxene formation and implications for granulite genesis. *Journal of Petrology* **43**, 2121–2141.

Nandakumar, V. & Harley, S. L. (2000). A reappraisal of the pressure–temperature path of granulites from the Kerala Khondalite Belt, southern India. *Journal of Geology* **108**, 687–703.

Newton, R. C., Smith, J. V. & Windley, B. F. (1980). Carbonic metamorphism, granulites and crustal growth. *Nature* **288**, 45–50.

O'Hara, M. J. (1977). Thermal history of excavation of Archean gneisses from the base of the continental crust. *Journal of the Geological Society, London* **134**, 185–200.

Owen, J. V. & Erdmer, P. (1989). Metamorphic geology and regional geothermobarometry of a Grenvillian massif: the Long Range Inlier, Newfoundland. *Precambrian Research* **43**, 79–100.

Pan, Y., Fleet, M. E. & Williams, H. R. (1994). Granulite-facies metamorphism in the Quetico subprovince, north of Manitouwadge, Ontario. *Canadian Journal of Earth Sciences* **31**, 1427–1439.

Patiño-Douce, A. E. & Beard, J. S. (1995). Dehydration melting of biotite gneiss and quartz amphibolite from 3 to 15 kbar. *Journal of Petrology* **36**, 707–738.

Patiño-Douce, A. E. & Beard, J. S. (1996). Effects of P, f_{O_2} and Mg/Fe ratio on dehydration melting of model metagreywackes. *Journal of Petrology* **37**, 999–1024.

Patiño-Douce, A. E. & Harris, N. (1998). Experimental constraints on Himalayan anatexis. *Journal of Petrology* **39**, 689–710.

Patiño Douce, A. E., Humphreys, E. D. & Johnston, A. D. (1990). Anatexis and metamorphism in tectonically thickened continental crust exemplified by the Sevier hinterland, western North America. *Earth and Planetary Science Letters* **97**, 290–315.

Pattison, D. R. M. (1989). P–T conditions and the influence of graphite on pelitic phase relations in the Ballachulish aureole, Scotland. *Journal of Petrology* **30**, 1219–1244.

Pattison, D. R. M. (1991). Infiltration-driven dehydration and anatexis in granulite facies metagabbro, Grenville Province, Ontario, Canada. *Journal of Metamorphic Geology* **9**, 315–332.

Pattison, D. R. M. (1992). Stability of andalusite and sillimanite and the Al_2SiO_5 triple point: Constraints from the Ballachulish aureole, Scotland. *Journal of Geology* **100**, 423–446.

Pattison, D. R. M. (2003). Petrogenetic significance of orthopyroxene-free garnet + clinopyroxene + plagioclase-bearing metabasites with respect to the amphibolite and granulite facies. *Journal of Metamorphic Geology* **21**, 21–34.

Pattison, D. R. M. & Bégin, N. J. (1994*a*). Zoning patterns in orthopyroxene and garnet in granulites: implications for geothermometry. *Journal of Metamorphic Geology* **12**, 387–410.

Pattison, D. R. M. & Bégin, N. J. (1994*b*). Hierarchy of closure temperatures in granulites and the importance of an intergranular exchange medium (melt?) in controlling maximum Fe–Mg exchange temperatures. *Mineralogical Magazine* **58A**, 694–695.

Pattison, D. R. M. & Harte, B. (1991). Petrography and mineral chemistry of pelites. In: Voll, G., Topel, J., Pattison, D. R. M. & Seifert, F. (eds) *Equilibrium and Kinetics in Contact Metamorphism: the Ballachulish Igneous Complex and its Aureole*. Heidelberg: Springer, pp. 135–180.

Pattison, D. R. M. & Harte, B. (1997). The geology and evolution of the Ballachulish Igneous Complex and Aureole. *Scottish Journal of Geology* **33**, 1–29.

Perchuk, L. L., Safonov, O. G., Gerya, T. V., Fu, B. & Harlov, D. E. (2000). Mobility and melting of components in metasomatic transformation and partial melting of gneisses: an example from Sri Lanka. *Contributions to Mineralogy and Petrology* **140**, 212–232.

Percival, J. A. (1983). High-grade metamorphism in the Chapleau–Foleyet area, Ontario. *American Mineralogist* **68**, 667–686.

Percival, J. A. (1991). Granulite-facies metamorphism and crustal magmatism in the Ashuanipi Complex, Quebec–Labrador, Canada. *Journal of Petrology* **32**, 1261–1297.

Percival, J. A. & McGrath, P. H. (1986). Deep crustal history and tectonic history of the northern Kapuskasing uplift of Ontario: an integrated petrological–geophysical study. *Tectonics* **5**, 553–572.

Perkins, D., III & Chipera, S. J. (1985). Garnet–orthopyroxene–plagioclase–quartz barometry: refinement and application to the English River subprovince and the Minnesota River valley. *Contributions to Mineralogy and Petrology* **89**, 69–80.

Perkins, D., III., Essene, E. J. & Marcotty, L. A. (1982). Thermometry and barometry of some amphibolite–granulite facies rocks from the Otter Lake area, southern Quebec. *Canadian Journal of Earth Sciences* **19**, 1759–1774.

Peterson, J. W. & Newton, R. C. (1989). Reversed experiments on biotite–quartz–feldspar melting in the system KMASH: implications for crustal anatexis. *Journal of Geology* **97**, 465–485.

Peterson, J. W., Chacko, T. & Kuehner, S. M. (1991). The effects of fluorine on the vapor-absent melting of phlogopite + quartz: implications for deep crustal processes. *American Mineralogist* **76**, 470–476.

Pëto, P. (1976). An experimental investigation of melting relations involving muscovite and paragonite in the silica-saturated portion of the system K_2O–Na_2O–Al_2O_3–SiO_2–H_2O to 15 kb total pressure. In: *Progress in Experimental Petrology. United Kingdom Natural Environment Research Council, Progress Report of Research Supported by NERC* **4**, 41–45.

Philpotts, A. R. (1990). *Principles of Igneous and Metamorphic Petrology*. Englewood Cliffs, NJ: Prentice–Hall, 498 pp.

Piwinskii, A. J. (1968). Experimental studies of igneous rock series central Sierra Nevada Batholith, California. *Journal of Geology* **76**, 548–570.

Powell, R. (1983). Fluids and melting under upper amphibolite facies conditions. *Journal of the Geological Society, London* **140**, 629–633.

Raith, M., Srikantappa, C., Ashamanjari, K. G. & Spiering, B. (1990). The granulite terrane of the Nilgiri Hills (southern India): characterization of high grade metamorphism. In: Vielzeuf, D. & Vidal, Ph. (eds) *Granulites and Crustal Evolution*. Dordrecht: Kluwer Academic, pp. 339–365.

Raith, M., Karmakar, S. & Brown, M. (1997). Ultra-high-temperature metamorphism and multistage decompressional

evolution of sapphire granulites from the Palni Hill Ranges, southern India. *Journal of Metamorphic Geology* **15**, 379–399.

Ravindra Kumar, G. R. & Chacko, T. (1994). Geothermobarometry of mafic granulites and metapelite from the Palghat Gap, South India: petrologic evidence for isothermal uplift and rapid cooling. *Journal of Metamorphic Geology* **12**, 479–492.

Riciputi, L. R., Valley, J. W. & McGregor, V. R. (1990). Conditions of Archean granulite metamorphism in the Godthab–Fiskenaesset region, southern West Greenland. *Journal of Metamorphic Geology* **8**, 171–190.

Rollinson, H. R. (1981). Garnet–pyroxene thermometry and barometry in the Scourie gneisses, NW Scotland. *Lithos* **14**, 225–238.

Rushmer, T. (1991). Partial melting of two amphibolites: contrasting experimental results under fluid-absent conditions. *Contributions to Mineralogy and Petrology* **107**, 41–59.

Rushmer, T. (1993). Experimental high pressure granulites: some applications to natural mafic xenolith suites and Archean granulite terranes. *Geology* **21**, 411–414.

Sandiford, M. (1985). The metamorphic evolution of granulites at Fyfe Hills; implications for Archaean crustal thickness in Enderby Land, Antarctica. *Journal of Metamorphic Geology* **3**, 155–178.

Sandiford, M. & Powell, R. (1986). Pyroxene exsolution in granulites from Fyfe Hills, Enderby Land, Antarctica: evidence for 1000°C metamorphic temperatures in Archean continental crust. *American Mineralogist* **71**, 946–954.

Santosh, M. (1987). Cordierite gneisses of southern Kerala, India: petrology, fluid inclusions and implications for crustal uplift history. *Contributions to Mineralogy and Petrology* **96**, 343–356.

Santosh, M., Harris, N. B. W., Jackson, D. H. & Mattey, D. P. (1990). Dehydration and incipient charnockite formation: a phase equilibria and fluid inclusion study from South India. *Journal of Geology* **98**, 915–926.

Savage, D. & Sills, J. D. (1980). High pressure metamorphism in the Scourian of NW Scotland: evidence from garnet granulites. *Contributions to Mineralogy and Petrology* **74**, 153–163.

Schumacher, J. C., Hollocher, K. T., Robinson, P. & Tracy, R. J. (1990*a*). Progressive reactions and melting in the Acadian metamorphic high of central Massachusetts and southwestern New Hampshire, USA. In: Ashworth, J. R. & Brown, M. (eds) *High Temperature Metamorphism and Crustal Anatexis*. London: Unwin Hyman, pp. 272–315.

Schumacher, R., Schenk, V., Raase, P. & Vitanage, P. W. (1990*b*). Granulite facies metamorphism of metabasic and intermediate rocks in the Highland Series of Sri Lanka. In: Ashworth, J. R. & Brown, M. (eds) *High-temperature Metamorphism and Crustal Anatexis*. London: Unwin Hyman, pp. 235–271.

Sen, C. & Dunn, T. (1994). Dehydration melting of a basaltic composition amphibolite at 1·5 and 2·0 GPa: implications for the origin of adakites. *Contributions to Mineralogy and Petrology* **117**, 394–409.

Sen, S. K. & Bhattacharya, A. (1984). An orthopyroxene–garnet thermometer and its application to the Madras charnockites. *Contributions to Mineralogy and Petrology* **88**, 64–71.

Sheraton, J. W., Offe, L. A., Tingey, R. J. & Ellis, D. J. (1980). Enderby Land, Antarctica—an unusual Precambrian high-grade metamorphic terrain. *Journal of the Geological Society of Australia* **27**, 1–18.

Sills, J. D. (1984). Granulite facies metamorphism in the Ivrea Zone, NW Italy. *Schweizerische Mineralogische und Petrographische Mitteilungen* **64**, 169–191.

Sills, J. D., Ackermand, D., Herd, R. K., & Windley, B. F. (1983). Bulk composition and mineral parageneses of sapphirine-bearing rocks along a gabbro–lherzolite contact at Finero, Ivrea Zone, N. Italy. *Journal of Metamorphic Geology* **1**, 337–351.

Spear, F. S. (1981). An experimental study of hornblende stability and compositional variability in amphibolite. *American Journal of Science* **281**, 697–734.

Spear, F. S. (1993). *Metamorphic Phase Equilibria and Pressure–Temperature–Time Paths*. *Mineralogical Society of America Monograph* **1**, 799 pp.

Spear, F. S. & Florence, F. P. (1992). Thermobarometry in granulites: pitfalls and new approaches. In: van Reenan, D. D., Roering, C., Ashwal, L. D. & de Wit, M. J. (eds) *The Archean Limpopo Granulite Belt: Tectonics and Deep Crustal Processes*. *Precambrian Research* **55**, 209–241.

Spear, F. S. & Markussen, J. C. (1997). Mineral zoning, *P–T–X–M* phase relations, and metamorphic evolution of some Adirondack granulites, New York. *Journal of Petrology* **38**, 757–783.

Spear, F. S., Kohn, M. J. & Cheney, J. T. (1999). *P–T* paths from anatectic pelites. *Contributions to Mineralogy and Petrology* **134**, 17–32.

Speer, J. A. (1982). Metamorphism of the pelitic rocks of the Snyder Group in the contact aureole of the Kiglapait layered intrusion, Labrador: effects of buffering partial pressures of water. *Canadian Journal of Earth Sciences* **19**, 1888–1909.

Srikantappa, C., Raith, M. & Spiering, B. (1985). Progressive charnockitization of a leptynite–khondalite suite in southern Kerala, India—evidence for formation of charnockites through a decrease in fluid pressure? *Journal of the Geological Society of India* **26**, 859–872.

Srikantappa, C., Raith, M. & Touret, J. L. R. (1992). Synmetamorphic high-density carbonic fluids in the lower crust: evidence from the Nilgiri Granulites, Southern India. *Journal of Petrology* **33**, 733–760.

St-Onge, M. R. & Lucas S. B. (1995). Large-scale fluid infiltration, metasomatism and re-equilibration of Archaean basement granulites during Palaeoproterozoic thrust belt construction, Ungava Orogen, Canada. *Journal of Metamorphic Geology* **13**, 509–535.

Stevens, G., Clemens, J. D. & Droop, G. T. R. (1997). Melt production during granulite-facies anatexis: experimental data from 'primitive' metasedimentary protoliths. *Contributions to Mineralogy and Petrology* **128**, 352–370.

Thompson, A. B. (1982). Dehydration melting of pelitic rocks and the generation of H_2O-undersaturated granitic liquids. *American Journal of Science* **282**, 1567–1595.

Thompson, A. B. (1990). Heat, fluids and melting in the granulite facies. In: Vielzeuf, D. & Vidal, Ph. (eds) *Granulites and Crustal Evolution*. Dordrecht: Kluwer Academic, pp. 37–58.

Thomson, J. A. (2001). A counterclockwise *P–T* path for anatectic pelites, south–central Massachusetts. *Contributions to Mineralogy and Petrology* **141**, 623–641.

Thost, D. E., Hensen, B. J. & Motoyoshi, Y. (1991). Two-stage decompression in garnet-bearing mafic granulites from Sostrene Island, Prydz Bay, East Antarctica. *Journal of Metamorphic Geology* **9**, 245–256.

Todd, C. S. & Evans, B. E. (1994). Properties of CO_2-induced dehydration of amphibolite. *Journal of Petrology* **35**, 1213–1239.

Turner, F. J. (1981). *Metamorphic Petrology*, 2nd edn. New York: McGraw–Hill.

Tuttle, O. F. & Bowen, N. L. (1958). Origin of granite in the light of experimental studies in the system $NaAlSi_3O_8$–$KAlSi_3O_8$–SiO_2–H_2O. *Geological Society of America, Memoirs* **74**, 54–63.

Valley, J. W., Bohlen, S. R., Essene, E. J. & Lamb, W. (1990). Metamorphism in the Adirondacks: II. The role of fluids. *Journal of Petrology* **31**, 555–596.

Vielzeuf, D. & Clemens, J. D. (1992). The fluid-absent melting of phlogopite + quartz: experiments and models. *American Mineralogist* **77**, 1206–1222.

Vielzeuf, D. & Montel, J. M. (1994). Partial melting of metagreywackes. Part I. Fluid-absent experiments and phase relationships. *Contributions to Mineralogy and Petrology* **117**, 375–393.

White, R. W., Powell, R., Holland, T. J. B. & Worley, B. A. (2000). The effect of TiO_2 and Fe_2O_3 on metapelitic assemblages at greenschist and amphibolite conditions: mineral equilibria calculations in the system K_2O–FeO–MgO–Al_2O_3–SiO_2–H_2O–TiO_2–Fe_2O_3. *Journal of Metamorphic Geology* **18**, 497–512.

White, R. W., Powell, R. & Holland, T. J. B. (2001). Calculation of partial melting equilibria in the system Na_2O–CaO–K_2O–FeO–MgO–Al_2O_3–SiO_2–H_2O (NCKFMASH). *Journal of Metamorphic Geology* **19**, 139–153.

Winther, K. T. & Newton, R. C. (1991). Experimental melting of hydrous low-K tholeiite: evidence on the origin of Archaean cratons. *Bulletin of the Geological Society of Denmark* **39**, 213–228.

Wodicka, N., Ketchum, J. W. F. & Jamieson, R. A. (2000). Grenvillian metamorphism of monocyclic rocks, Georgian Bay, Ontario, Canada: implications for convergence history. *Canadian Mineralogist* **38**, 471–510.

Wood, B. J. (1976) The reaction phlogopite + quartz = enstatite + sanidine + H_2O. *United Kingdom Water and Environmental Resources Council – Progress in Experimental Petrology* **6**, 17–19.

Xishan, L., Wei, J., Shuxun, L. & Xuechun, X. (1993). Two types of Precambrian high-grade metamorphism, Inner Mongolia, China. *Journal of Metamorphic Geology* **11**, 499–510.

Yardley, B. W. D. (1989). *An Introduction to Metamorphic Petrology*. Harlow: Longman, 248 pp.

Yund, R. A. (1986). Interdiffusion of NaSi–CaAl in peristerite. *Physics and Chemistry of Minerals* **13**, 11–16.

SUPPLEMENTARY DATA

Supplementary data for this paper are available on *Journal of Petrology* online.

APPENDIX: LOCALITIES, SAMPLES AND REFERENCES

Locality and samples	Reference(s)	Regional/contact	Type*
Adirondack Highlands, NY	Bohlen & Essene (1979; 1980)	R	M
11 *AS3, BM13, BM2, ET1, ET15, ET24, IN11, N3, S15, SR29, SR31*			
Adirondack Lowlands, NY	Edwards & Essene (1988)	R	I
1 *RS34*			
Agto, W. Greenland	Glassley & Sorensen (1980)	R	M
3 *88589, 91154, 91156*			
Akia, W. Greenland	Griffin *et al*. (1980)	R	M
3 *152735, 152733, 152765*			
Akia, W. Greenland	Riciputi *et al*. (1990)	R	I
3 *266935, 341925, 341965*			
Arendal, Norway	Lamb *et al*. (1986)	R	M
6 *B750, C7652, C814, C815, D714, D7606*			
Ashuanipi, Quebec	Percival (1991)	R	I
10 *27, 47, 96, 98, 142, 152, 216, 262, 266, 347*			
Bahai, Brazil	Ackermand *et al*. (1987)	R	A
1 *CAR-19*			
Ballachulish, Scotland	Pattison (1989 and unpublished)	C	A
2 *568-1, 568-2*			
Bengal, E. India	Bhattacharya & Mukherjee (1987)	R	M
2 *SM-4b, SM-44b*			
Cone Peak, California	Hansen & Stuk (1993)	R	M
6 *82G4t, 87G2, 87G3, 87G4, H2a, H3*			
Dronning Maud Land, E. Antarctica	Bucher-Nurminen & Ohta (1993)	R	I
1 *KBN-702*			
Eifel, Germany	Loock *et al*. (1990)	R	M
4 *EIF-S1, EIF-S16, EIF-S35, EIF-S37*			
Enderby Land, Antarctica	Harley (1985); Harley *et al*. (1990)	R	I/A
25 *49659, 3411, 3423, 3468, 3532, 3552, 3597, 3964, 3970, 3973, 4003, 4528, 4547, 4549, 4593, 4833, 49382, 49657, 49734, 49740, 49748, 49749, 49891, 4648, 4652*			

Appendix: continued

Locality and samples	Reference(s)	Regional/contact	Type*
English River, Ontario	Perkins & Chipera (1985)	R	I
7 *ID1683, G1a, G63B, RW1283, BL1083, CL2283, HS1583*			
Fiordland, New Zealand	Bradshaw (1989*a*)	R	M
1 *51112*			
Furua Complex, Tanzania	Coolen (1980)	R	M
16 *1, 2, 4, 5, 6, 11, 22, 23, 25, 26, 28, 33, 49, 55, 91, 94*			
Ganguvarpatti, S. India	Mohan & Windley (1993)	R	I
3 *97-127, 97125-40, 97125-86*			
Grenville Province, Ontario	Anovitz & Essene (1990)	R	M
8 *BA-9A, 83C6, 83C5, 83C70, 83C9, 85A12, 83C15, 83C19*			
Grenville Prov. (Georgian Bay), Ont.	Wodicka *et al*. (2000)	R	A/M
2 *N131a, N153c*			
Grenville Prov. (Huntsville), Ont.	Pattison (1991)	R	M
3 *Hu1, P2-6-2b, Hu15a*			
Grenville Prov. (Otter Lake), Quebec	Perkins *et al*. (1982)	R	M/I
6 *AL2, DD11, DD17, DD12, RK1, RK2*			
Guaxupé, Brazil	Iyer *et al*. (1996)	R	M
2 *AC89, AC89s*			
Hidaka, Japan	Komatsu *et al*. (1994)	R	A
1 *HS412p2*			
Iforas, Mali	Boullier & Barbey (1988)	R	M/I
3 *IC-114a, IC115, IC115b*			
Ivrea Zone, Italy	Sills *et al*. (1983); Sills (1984)	R	I/M
4 *IVL, IV101, IV346, IV383*			
Jetty Peninsula, E. Antarctica	Hand *et al*. (1994)	R	A
1 *JT6665*			
Kapuskasing, Ontario	Percival (1983)	R	I
4 *PG13, PG16, PG21, PG22*			
Kapuskasing (North), Ontario	Percival & McGrath (1986)	R	I
6 *Kap-5, Kap-6, Kap-7, Kap-8, Kap-9, Kap-10*			
Karnataka-Tamil Nadu, S. India	Janardhan *et al*. (1982)	R	I/M
6 *11-1b, 11-3e, 11-1, GN-4a, 4-1c, 10-1a*			
Karnataka-Tamil Nadu, S. India	Hansen *et al*. (1987)	R	I
1 *T13-83*			
Kasai, Zaire	Bingen *et al*. (1988)	R	A
6 *12195, 139131, 139160, 73535, 139246, 139146*			
Kerala Khondalite Belt, S. India	Chacko *et al*. (1987, 1996 and unpublished)	R	I/A
17 *76-112, 96-136, 165-241, 77-115, 95-135, 45-84, 55-89, 83-123, 170-246, 177-260, 4-10a, 121-166, 141-201, 153-225, 154-226, 155-229, 147-217*			
Kerala Khondalite Belt, S. India	Harris *et al*. (1982)	R	I/A
4 *732, 758, 766, 770*			
Kerala Khondalite Belt, S. India	Hansen *et al*. (1987)	R	I
5 *K18-6a, K18-7, 147-214, TN3-1, TN21-4*			
Kerala Khondalite Belt, S. India	Nandakumar & Harley (2000)	R	I/A
3 *ED3, ED8, ED9*			
Kerala Khondalite Belt, S. India	Santosh (1987); Santosh *et al*. (1990)	R	A/I
2 *86-2, M-4*			

Locality and samples	Reference(s)	Regional/contact	Type*
Kerala Khondalite Belt, S. India	Srikantappa *et al*. (1985)	R	I
3 *23, 25, 36*			
Ketilidian Belt, S. Greenland	Dempster *et al*. (1991)	R/C	A/I
9 *A255, A289, A374, A375, A379, I65, Q62, Q64, Q67*			
Kiglapait, Labrador	Speer (1982)	C	A/I
2 *NC-49, SN-211*			
Laramie, Wyoming	Grant & Frost (1990)	C	A/I
3 *19-4a, 53-2b, 53-2c*			
Long Range Inlier, Nfld	Owen & Erdmer (1989)	R	I/A
3 *86-451-2, 86-111, 86-279*			
Madras Charnockites, S. India	Sen & Bhattacharya (1984)	R	I/M
8 *379, 558, 702, 715, 729, 403b, 543a, 79112*			
Magondi, N. Zimbabwe	Munyanyiwa *et al*. (1993)	R	M
3 *NY81-3, NY84-1, NY84-2*			
Makhavinekh, Labrador	McFarlane *et al*. (2003)	C	A
11 *M02-20, M15-250, M04-450, M05-800, M17-1015, M21-1500, M22-2025, M23-2400, M08-3125, M12-4025, T03-5750*			
Minnesota River, USA	Perkins & Chipera (1985)	R	I
5 *GF3-8, GF3-6, GF5-4, GF5-3, GF5-2*			
Minto, Quebec	Bégin & Pattison (1994*a*);	R	I/A
6 *B69E, C10B, P88, B58, B74b, P69*	Pattison & Bégin (1994)		
Molodezhnaya, Antarctica	Grew (1981)	R	I
3 *322, 322a, 341b*			
Inner Mongolia, China	Xishan *et al*. (1993)	R	M
2 *MONGO010, MONGO691*			
Nain, Labrador	Berg (1977*a*, 1977*b*)	C/R	A
16 *LRD72, KI3909, KI3557, 2-893, 2-625, 2-1833, 2-275, RAW437, NU69, NK420b, 74-98, 2-1726, 2-1637, KI3911, 74-16b, 74-18x*			
Nilgiri Hills, S. India	Srikantappa *et al*. (1992)	R	I/M
11 *78, 85, 88, 95, 110, 182, 304, 314, 337, KU4, KU7*			
Nilgiri Hills, S. India	Raith *et al*. (1990)	R	M/I
51 *2, 3, 4, 5, 6, 7, 8, 10, 11, 12, 13, 15, 18, 19, 20, 22, 31, 32, 33, 34, 35, 36, 37, 38, 39, 40, 41, 42, 43, 44, 45, 46, 47, 48, 49, 50, 51, 52, 53, 54, 55, 56, 57, 58, 61, 64, 65, 68, 72, 76, 78*			
Paderu, S. India	Lal *et al*. (1987)	R	A
3 *252, 259, 320*			
Palghat Gap, S. India	Ravindra Kumar & Chacko (1994)	R	M
4 *112, 112a, 122, 170*			
Palni Hills, S. India	Raith *et al*. (1997)	R	A
1 *PH-172b*			
Pikwitonei, Manitoba	Arima & Barnett (1984)	R	A
2 *PIKPO4a1, PIKPO4b*			
Prydz Bay, Antarctica	Fitzsimons & Harley (1994)	R	I
16 *88/118, 89/71, 89/63, 89/59, 89/334, 89/2, 89/108, 88/88, 88/65, 88/50, 88/41, 88/38, 88/333, 88/168, 89/40, 89/106*			
Prydz Bay, E. Antarctica	Thost *et al*. (1991)	R	M
1 *8813001*			
North Quetico, Ontario	Percival & McGrath (1986)	R	I
6 *Q-1, Q-2, Q-4, Q-5, Q-6, Q-7*			

Appendix: continued

Locality and samples	Reference(s)	Regional/contact	Type*
S.-Central Quetico, Ontario	Pan *et al*. (1994)	R	I
3 *YP01B, G409, G2229*			
Rauer Group, E. Antarctica	Harley & Fitzsimons (1991)	R	I
3 *88-335, 65768c, 88-218a*			
San Gabriel, S. California	Barth & May (1992)	R	M
4 *273b, CB86-1a, CB88-5, CC83-157*			
NE Scotland	Ashworth & Chinner (1978); Droop & Charnley (1985)	C	A
5 *BELHM5, BELSP1d, HP105570, HP82891, HPCB1*			
Scourie, Scotland	Savage & Sills (1980); Rollinson (1981)	R	M/I
2 *SCOUR84, 275*			
Highland Series, Sri Lanka	Schumacher *et al*. (1990*b*)	R	M/I
10 *K130-1, K144-4, K1-5, K200, K242-2, K302, K355-1, K408, K460-1, K50-1*			
Highland Series, Sri Lanka	Hansen *et al*. (1987)	R	I
1 *D4-N2*			
Sveconorwegian Belt, Sweden	Johansson *et al*. (1991)	R	M
2 *HALLANDSAS, TYLOSAND*			
Taltson, NWT	Berman & Bostock (1997)	R	I/A
15 *106b, 145b, 187c, 2063a, 223b, 258a, 310a, 317a, 353a, 40a, 505b, 59a, 59b, 718a, 96b*			
Tasiusarsuaq, W. Greenland	Riciputi *et al*. (1990)	R	M
2 *6728-22, 6728-27*			
Torngat, Labrador	Mengel & Rivers (1991, 1997)	R	M/I
3 *F84-110, MZ-194, 25b*			
Ungava, Quebec	St-Onge & Lucas (1995)	R	M
1 *UNGD-192*			
Val Rita, Ontario	Percival & McGrath (1986)	R	I
5 *VR-1, VR-2, VR-3, VR-4, VR-5*			

Total: 414 samples.
*M, mafic; I, intermediate; A, aluminous.